# STEAM REFORMING OF ETHANOL OVER SOL-GEL-SYNTHESIZED MIXED OXIDE CATALYSTS

A THESIS SUBMITTED TO
THE GRADUATE SCHOOL OF NATURAL AND APPLIED SCIENCES
OF
MIDDLE EAST TECHNICAL UNIVERSITY

BY

HAKAN ÖNDER OLCAY

IN PARTIAL FULFILLMENT OF THE REQUIREMENTS
FOR
THE DEGREE OF MASTER OF SCIENCE
IN
CHEMICAL ENGINEERING

JULY 2005

Approval of the Graduate School of Natural and Applied Sciences

_____

Prof. Dr. Canan ÖZGEN

Director

I certify that this thesis satisfies all the requirements as a thesis for the degree of Master of Science.

_____

Prof. Dr. Nurcan BAÇ

Head of Department

This is to certify that I have read this thesis and that in my opinion it is fully adequate, in scope and quality, as a thesis for the degree of Master of Science

_____

Prof. Dr. Deniz ÜNER

Supervisor

| | | |
|---|---|---|
| Prof. Dr. Ali ÇULFAZ | (METU, ChE) | _____ |
| Prof. Dr. Deniz ÜNER | (METU, ChE) | _____ |
| Dr. N. Alper TAPAN | (Gazi Univ., ChE) | _____ |
| Kemal DEMİRKOL | (TTGV) | _____ |
| Assist. Prof. Dr. Ayşen YILMAZ | (METU, Chem) | _____ |

**I hereby declare that all information in this document has been obtained and presented in accordance with academic rules and ethical conduct. I also declare that, as required by these rules and conduct, I have fully cited and referenced all material and results that are not original to this work.**

Name, Last Name : Hakan Önder OLCAY

Signature :

# ABSTRACT

STEAM REFORMING OF ETHANOL
OVER SOL-GEL-SYNTHESIZED MIXED OXIDE CATALYSTS

Olcay, Hakan Önder
M.S., Department of Chemical Engineering
Supervisor : Prof. Dr. Deniz Üner

July 2005, 91 pages

Depletion in the reserves of fossil fuels, inefficient energy production from these fuels and the negative effect of their usage on atmosphere, and thereby, on human health have accelerated researches on clean energy. Hydrogen produced from ethanol when used in fuel cells not only generates efficient energy but also creates a closed carbon cycle in nature.

ZnO and Cu/ZnO catalysts are known with their superior performance in alcohol synthesis. From the principle of microkinetic reversibility they are expected to be superior catalysts for the steam reforming reaction of ethanol as well. ZnO catalysts can be modified by precious, Pd, or non-precious, Cu, metals to enhance hydrogen desorption capability, and dispersed on $SiO_2$ for high surface areas via sol-gel technique.

Steam reforming tests over ZnO catalysts revealed that they act only as ethanol dehydrogenation catalysts in the temperature range of 300-500°C. Promotion with Pd or Cu decreased hydrogen selectivity due most probably to unreachable closed pores of the catalysts. Autothermal reforming tests over both $ZnO/SiO_2$

and Co/SBA-15 catalysts, on the other hand, gave rise to the formation of several side products.

Keywords: Ethanol Steam Reforming, Palladium, Copper, Zinc Oxide, Cobalt

# ÖZ

SOL-JEL İLE HAZIRLANMIŞ KARIŞIK OKSİT KATALİZÖRLER ÜZERİNDE ETANOLÜN BUHAR RİFORMLAMASI

Olcay, Hakan Önder
Yüksek Lisans, Kimya Mühendisliği Bölümü
Tez Yöneticisi : Prof. Dr. Deniz Üner

Temmuz 2005, 91 sayfa

Fosil yakıt yataklarındaki azalma, bu yakıtlardan elde edilen enerjinin verimsiz oluşu, ve bunların kullanımının atmosfer ve insan sağlığı üzerindeki olumsuz etkisi temiz enerji konulu araştırmalara ivme kazandırmıştır. Etanolden üretilen hidrojen yakıt hücrelerinde kullanıldığında hem verimli enerji üretilmekte hem de doğada kapalı bir karbon çevrimi oluşturulmaktadır.

ZnO ve Cu/ZnO katalizörler alkol sentezlemedeki üstün performanslarıyla bilinirler. Mikrokinetik tersinirlik prensibine dayanarak bu katalizörlerin etanol buhar riformlaması tepkimesinde de etkin rol oynayacağı düşünülmektedir. Sol-jel tekniğiyle ZnO katalizörlerin hidrojen dezorplama yeteneğini artırmak amacıyla Pd gibi değerli metallerle veya Cu gibi değerli olmayan metallerle yapısı değiştirilebilir, ve bu katalizörler yüksek yüzey alanı sağlama amacıyla $SiO_2$ üzerine dağıtılabilir.

ZnO katalizörler üzerinde 300-500°C sıcaklıklarda gerçekleştirilen buhar riformlaması deneyleri bu katalizörlerin sadece etanolden hidrojen koparmaya yardımcı olduğunu göstermiştir. Pd veya Cu eklenmiş katalizörlerde yapılarında bulunan olası kapalı gözeneklerin bir sonucu olarak daha az hidrojen seçiciliği

elde edilmiştir. $ZnO/SiO_2$ ve Co/SBA-15 katalizörler üzerinde oksijen ortamında gerçekleştirilen düzeltim deneylerinde ise bir dizi yan ürün dağılımı elde edilmiştir.

Anahtar Kelimeler: Etanol buhar riformlaması, Paladyum, Bakır, Çinko oksit, Kobalt

To My Grandma

# ACKNOWLEDGMENTS

I would like to thank Prof. Dr. Deniz Üner for her guidance, suggestions, encouragements and valuable comments throughout this study.

I would also like to acknowledge Assist. Prof. Dr. Erol Şeker and Işıl Tezel at Izmir Institute of Technology, Assist. Prof. Dr. Ayşen Yılmaz at Chemistry Department, and my friends, Burcu and Mukaddes for synthesizing the catalysts and carrying out part of their characterization tests.

I want to extend my thanks to Prof. Dr. İnci Eroğlu for lending us their chiller which is used to provide cold stream to the coolers in the experimental setup, and Prof. Dr. Timur Doğu for letting us use their GC calibration gas.

I also wish to express my great appreciation to the members of CaCTUS group, and my friends, Aslı, Belma, Berker, Bilge, Canan, Ela, Hande, Serdar, Sezen and Zeynep for their irreplaceable encouragement, good humor and partnership. I must also say a special thank you to my high school friends for their deepest friendship, and another special thank you to Umut for inciting me to prepare the thesis format far long time ago.

I also want to express my gratitude to Ms. Gülten Orakçı, Ms. Mihrican Açıkgöz, Ms. Kerime Güney, and the personnel of machine workshop of Chemical Engineering Department for their technical assistance.

Finally, I would like to send my greatest gratitudes to my beloved family.

This study was supported by the METU Institute of Natural and Applied Sciences Grant No: BAP-2004-07-02-00-99, and by TÜBİTAK MİSAG-241. TÜBİTAK BAYG is kindly appreciated for the M.S. scholarship.

# TABLE OF CONTENTS

APPENDICES

# LIST OF TABLES

TABLES

# LIST OF FIGURES

FIGURES

# CHAPTER 1

# INTRODUCTION

World's energy consumption depends largely on fossil fuels. More than 85% of energy consumed in the last decade was obtained from fossil fuels [1]. Figure 1 illustrates the world primary energy consumption by energy source for years 1970-2001 and with predictions up to 2025.

In 1956 M. King Hubbert, a geologist with Shell Oil, observed that unrestrained extraction of a finite resource rises along a bell-shaped curve which gives peak when about half the resource is gone. Based on his theory, by 2060s petroleum will be exhausted [3]. Today there is still an increasing demand for oil the widespread usage of which in the transportation sector contributes to serious environmental problems. As an immediate precaution automobile industry has put into operation the usage of catalytic converters on both gasoline-fueled and diesel-fueled engines, and particulate filters on diesel-fueled engines which helped the emission values to decrease in one automobile; however, total emission values continued to increase upon increasing demand [1,4]. Figure 2 illustrates world energy-related carbon dioxide emissions by fuel type from 1970 to 2001, and also presents predictions until 2025 if no further precautions are taken. According to Kyoto Protocol signed in 1997 many countries agreed on reducing their overall emissions of six greenhouse gases ($CO_2$, $CH_4$, $N_2O$, HFCs, PFCs and $SF_6$) by at least 5% below 1990 levels over the period between 2008 and 2012 [5].

Both decrease in fossil fuel reserves and new regulations on emission control lead the way to the development of new engines and alternative fuels like

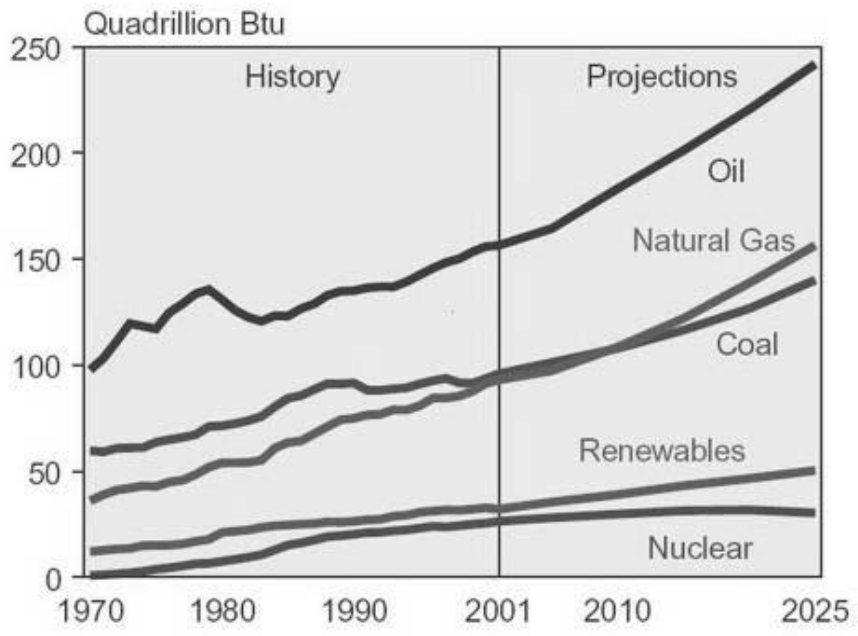


***Figure 1.*** *World primary energy consumption by energy source [1,2]*

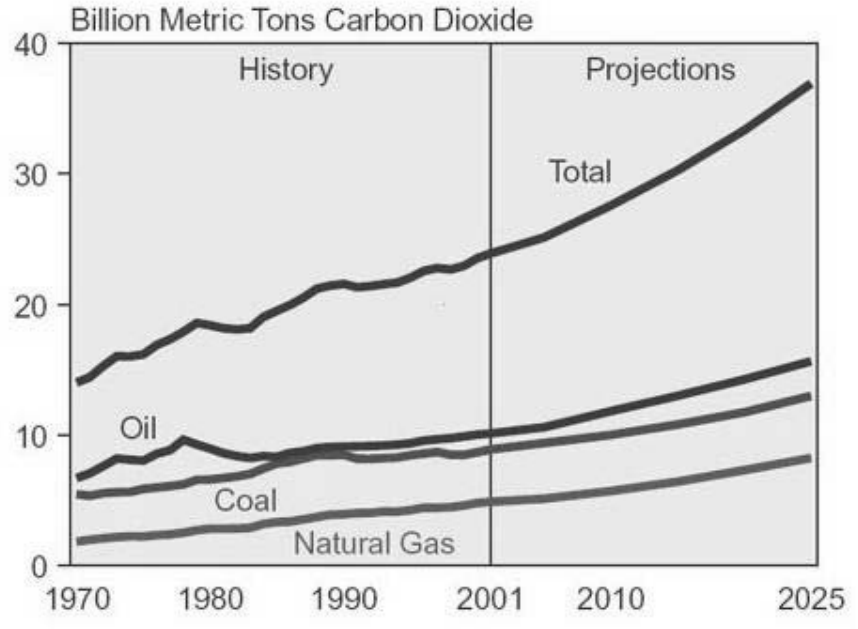


***Figure 2.*** *World energy-related carbon dioxide emissions by fuel type [1,2]*

hydrogen. Hydrogen can be derived from carbonaceous materials, e.g. hydrocarbons, and/or water through electrolysis, steam reforming, thermal dissociation or partial oxidation [6]. Biomass gasification or reforming arose as new areas of research.

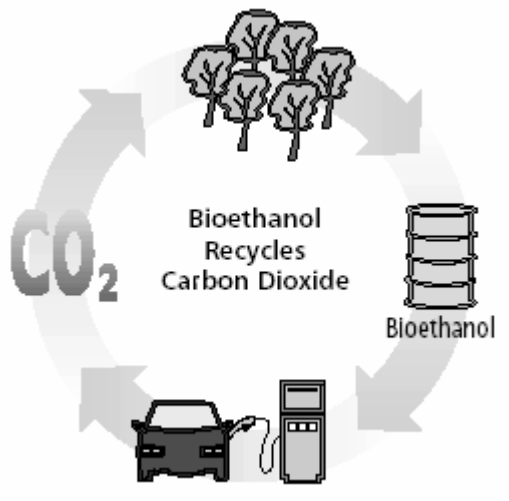


***Figure 3.*** *Closed carbon cycle [8]*

Sugar, starch, oils and crop wastes have been used as biomasses for hydrogen generation; however, their usage has been limited either by low hydrogen selectivities or by their high costs [7]. Ethanol is now another candidate. Hydrogen produced from especially bioethanol[1] when used in fuel cells for electricity generation creates a closed carbon cycle in nature releasing no additional carbon dioxide [8]. This closed carbon cycle is illustrated in Figure 3.

[1] Bioethanol is an aqueous solution containing ca. 12wt% ethanol.

Hydrogen can be produced from ethanol either by steam reforming or by direct partial oxidation:

$$C_2H_5OH + H_2O \leftrightarrow 2CO + 4H_2 \qquad \Delta H_R^o = +256\,kJ/mol \tag{1}$$

$$C_2H_5OH + \tfrac{1}{2}O_2 \leftrightarrow 2CO + 3H_2 \qquad \Delta H_R^o = +14\,kJ/mol \tag{2}$$

These reactions are followed by water-gas shift reaction:

$$CO + H_2O \leftrightarrow CO_2 + H_2 \qquad \Delta H_R^o = -41\,kJ/mol \tag{3}$$

Heat needs to be supplied either externally or internally to the system as both of the reactions (1) and (2) are endothermic. Therefore, partial oxidation reaction cannot take place without some external heat or without some total oxidation:

$$C_2H_5OH + 3O_2 \leftrightarrow 2CO_2 + 3H_2O \qquad \Delta H_R^o = -1277\,kJ/mol \tag{4}$$

Heat generated by total oxidation reaction can also be used for steam reforming case. This time a combination of steam reforming reaction with partial and total oxidation reactions are under consideration along with the water-gas shift reaction:

$$C_2H_5OH + 2H_2O + \tfrac{1}{2}O_2 \leftrightarrow 2CO_2 + 5H_2 \qquad \Delta H_R^o = -68\,kJ/mol \tag{5}$$

This reaction is named as indirect partial oxidation or autothermal reaction [7,9].

In this study, sol-gel-synthesized supported zinc oxide and cobalt catalysts were tested for their activities and selectivities towards hydrogen in ethanol steam reforming and autothermal reforming.

Deluga et al. [7] have presented a simple economic analysis of autothermal ethanol reforming for producing hydrogen for fuel cells. They considered a

totally idealized cycle starting from formation of glucose by photosynthesis and ending up in a fuel cell through ethanol fermentation from glucose and autothermal reforming of ethanol. They carried out the analysis taking only the reaction enthalpies into account. Assuming an ethanol cost of $1 per gallon, they arrived at a fuel cost of $0.04 per kWh. This value also applies for ethanol steam reforming as this idealized system consists of same species for both reforming cases.

An economic analysis similar to that of Deluga et al. [7], however, that rely on a more realistic model was also carried out in this study. A fuel cost of $0.09 per kWh was obtained at the end for both steam reforming and autothermal reforming cases. This value in fact decreases the annual fuel cost of a gasoline vehicle by more than a factor of two when compared with a hydrogen fuel cell vehicle [10]. Details of this analysis are given in Appendix A.

The next chapter, Chapter 2, reviews the literature about studies on hydrogen production from alcohols as well as on alcohol synthesis. Thermodynamics of alcohol-water systems were also discussed in that chapter. Chapter 3, on the other hand, describes the details of the experimental work carried out. Results of this work are given in Chapter 4 along with comments and discussions. Following two chapters, Chapters 5 and 6, lastly summarizes and arrives at conclusions, and gives some recommendations, respectively.

# CHAPTER 2

# LITERATURE SURVEY

Besides being a biomass, ethanol is an alcohol. Reverse of the ethanol steam reforming reaction (Reaction (1)) is nothing but ethanol synthesis from syngas. Therefore, starting literature survey with alcohol synthesis studies would be very well appropriate. In the second part, studies on reaction thermodynamics of ethanol-water systems will be explained. The rest of this chapter will be on various papers dealing with steam reforming of ethanol and methanol, and possible side reactions.

## 2.1. Lower and Higher Alcohol Synthesis

Catalysts are substances that change the reaction rate by promoting a different mechanism for the reaction without being consumed in the reaction. As they decrease the activation energy barrier of the reaction, from the principle of microkinetic reversibility, they also decrease the activation energy barrier for the reverse of that reaction. In this respect, it may be expected for a good higher alcohol synthesis catalyst also to be a good steam reforming catalyst.

Claus et al. [11] listed the routes for ethanol synthesis available in literature. According to their analysis, there are mainly four economically attractive routes to ethanol:

1. Ethylene hydration: $C_2H_4 + H_2O \leftrightarrow C_2H_5OH$
2. Hydrocarbonylation of methanol: $CH_3OH + CO + H_2O \leftrightarrow C_2H_5OH + O_2$
3. Synthesis from syngas: $CO + 2H_2 \leftrightarrow CH_3OH$

4. Hydrogenolysis of acetate

It is known that acetate production takes place in two steps:

- Methanol carbonylation to acetic acid: $CH_3OH + CO \leftrightarrow CH_3COOH$
- Esterification of acetic acid with methanol or ethanol:
  $CH_3COOH + CH_3OH \leftrightarrow CH_3COOCH_3 + H_2O$ or,
  $CH_3COOH + CH_3CH_2OH \leftrightarrow CH_3C(O)OCH_2CH_3 + H_2O$

Claus et al. have studied the selective hydrogenolysis of methyl and ethyl acetate to ethanol over different copper-based and supported Group VIII metal (Pd, Rh, Pt, Co, Ni) catalysts (CuO/MgO-$SiO_2$, CuO/ZnO/$Fe_2O_3$, CuO/ZnO, CuO/$Al_2O_3$-$SiO_2$, CuO/ZnO/MnO/$Al_2O_3$, Co/$TiO_2$, Co-Rh/$TiO_2$, Co-Rh-Fe/$TiO_2$, Co-Rh-Cu/$TiO_2$, Ni/$SiO_2$, Pd/$Al_2O_3$, Zn-Pd/$Al_2O_3$, Rh on activated carbon, Rh/$Al_2O_3$, Pt/$Al_2O_3$, Co/$TiO_2$, Co-Rh-Cu/$TiO_2$) in the gas phase at 448-623 K and 0.1-6.0 MPa. Over copper catalysts, they proposed the following reaction mechanism to take place:

I. $CH_3COOCH_3 + 2H_2 \leftrightarrow CH_3CH_2OH + CH_3OH$

II. $CH_3COOCH_3 + CH_3CH_2OH \leftrightarrow CH_3COOCH_2CH_3 + CH_3OH$

III. $CH_3COOCH_2CH_3 + H_2 \leftrightarrow C_2H_4O + CH_3CH_2OH$

IV. $C_2H_4O + H_2 \leftrightarrow CH_3CH_2OH$

Product distribution for Cu catalysts contains ethanol, methanol, ethyl acetate and above 260°C, methane and ethane. It is the CuO/MgO-$SiO_2$ catalyst showing the best result in ethanol synthesis as the basic MgO helps creation of electron-rich copper sites.

Addition of Fe and Mn to the catalysts promotes ethanol synthesis changing the side product distribution a little bit. For instance, over iron-promoted

$CuO/ZnO/MnO/Al_2O_3$ catalyst, acetaldehyde, 2-butanone, butanal, butanol, butyl acetate and acetone were obtained.

Bimetallic catalysts and all Cu catalysts except $CuO/Al_2O_3$-$SiO_2$, which showed deactivation above 260°C, exhibit high activity and selectivity (98%). Increase of temperature and pressure also promoted the ethanol and methanol selectivities.

From the kinetics point of view, comparison of turnover frequencies showed that acetaldehyde is more rapidly hydrogenated. Also, hydrogenolysis of ethyl acetate proceeds faster than that of methyl acetate. It is further shown that over $CuO/MgO$-$SiO_2$ catalyst reaction orders with respect to methyl acetate and hydrogen (Reaction I in the above mechanism), methyl acetate and ethanol (II), and ethyl acetate and hydrogen (III and IV) are all equal to one.

Product distributions obtained over Group VIIIB metal catalysts are summarized in Table 1 below.

***Table 1.*** *Product distributions obtained for methyl acetate hydrogenolysis over Group VIIIB metal catalysts of the study by Claus et al. [11]*

| **Catalyst** | **Product Distribution** |
|---|---|
| $Ni/SiO_2$ | Methane, ethane, $CO_x$, acetic acid |
| $Pd/Al_2O_3$ | Ethyl acetate |
| $Zn$-$Pd/Al_2O_3$ | Ethanol |
| Rh/Activated Carbon | Acetic acid, methane, ethane |
| $Rh/Al_2O_3$ | Methane, ethane, acetic acid, ethanol, ethyl formate, diethyl ether |
| $Pt/Al_2O_3$ | Ethanol, ethane, diethyl ether |

No activity was observed on $Pd/Al_2O_3$ whereas over monometallic catalysts comprising Rh, Pt and Ni, the hydrogenolysis of ethyl acetate is a nonselective reaction. As a note, formation of diethyl ether over alumina supported catalysts results from alcohol dehydration on acidic alumina.

Finally, $Co/TiO_2$ catalyst exhibited high activity and selectivity towards ethanol. Addition of Rh decreases selectivity due to formation of oxygenates; however, further addition of Fe increased ethyl acetate conversion. On the other hand, $Co-Rh-Cu/TiO_2$ performed poor results.

Nunan et al. [12,13] have investigated the effect of Cs/Cu/ZnO and $Cs/Cu/ZnO/Me_2O_3$ catalysts (Me = Cr, Al, Ga) with different Cs amounts on higher alcohol synthesis at 583 K, 7.6 MPa and with $H_2/CO = 0.45$ synthesis gas at GHSV = 5330 liters (STP)/kg cat/h.

Alumina and chromia are commercial supports because all practical industrial methanol synthesis catalysts are supported with alumina and chromia. They increase the surface area and stability of the catalyst, and therefore, they are structural promoters. They also induce the formation of side products like dimethyl ester (which can also be inhibited by Cs doping) and hydrocarbons.

Addition of cesium promotes methanol synthesis and water-gas shift reaction, as well as, the formation of ethanol and methyl formate. Alumina causes occlusion of cesium by burying cesium into bulk so that C-C bonds cannot be made. As a result over alumina supported cesium catalysts methanol is synthesized as the only major alcohol. On the other hand, presence of alumina support promotes total alcohol selectivity (for the case of Cs doped catalysts, in other words, methanol selectivity). Chromia, alternatively, promotes especially higher alcohol synthesis bearing no effect on the mechanism. When Cs is doped on the chromia supported catalyst, selectivities to branched alcohols like 1-propanal, 2-methyl-1-propanol, 2-methyl-1-butanol are affected.

Effect of cesium on higher alcohol synthesis mechanism was probed by $^{13}C$ nuclear magnetic resonance (NMR) analysis. Results showed that over Cu/ZnO catalysts higher alcohols are synthesized by linear insertion chain growth,

$$CH_3{}^{13}CH_2OH \xrightarrow{CO/H_2} CH_3{}^{13}CH_2CH_2OH \quad (6)$$

whereas, over Cs/Cu/ZnO catalysts it is the β-carbon addition, which is also named as aldol coupling with oxygen retention reversal,

$$CH_3{}^{13}CH_2OH \xrightarrow{CO/H_2} {}^{13}CH_3CH_2CH_2OH \quad (7)$$

Cu/ZnO is a hydrogenation catalyst. Doping of cesium provides basic sites which prevents production of side products, which helps promoting higher alcohol synthesis. On the other hand, cesium blocks hydrogenation sites on the catalyst surface. Therefore, higher alcohol selectivity passes through a maximum as amount of cesium on the catalyst increases due to this bifunctional nature of the catalyst. Similarly, chromia has an acidic nature which promotes higher alcohol synthesis, and ester production (Klier et al. [14]). However, in order to prevent formation of side product which are also promoted by this acidity, Cs should be doped to bring some basicity.

Finally, product distribution obtained both over Cs/Cu/ZnO and Cs/Cu/ZnO/$Cr_2O_3$ are similar. Cs/Cu/ZnO/$Ga_2O_3$ is a poor methanol catalyst because Ga interacts with Cs.

Smith et al. [15] have developed a kinetic reaction network for the synthesis of oxygenates over Cs-promoted Cu/ZnO catalysts in a differential reaction regime. According to previous studies there are basically three mechanistic reaction paths for higher alcohol synthesis over Cs/Cu/ZnO that are dominant:

- Insertion of CO or a single-carbon ($C_1$) intermediate to yield linear alcohols (l)
- β-addition yielding 2-methyl-branched primary alcohols (β)
- Methyl ester formation by oxygen attachment of a C1 intermediate to the α-carbon of the lower alcohol (α)

These three reaction paths are illustrated in Figure 4.

Estimates of the kinetic parameters showed that the β-addition is faster than linear growth, which results in high selectivities to branched alcohols like 2-methyl-1-propanol. It was also found that the rate of growth of double-carbon ($C_2$) intermediate is faster than for any other $C_n$ ($n \geq 2$) intermediate, which is specific to Cs-promoted catalyst.

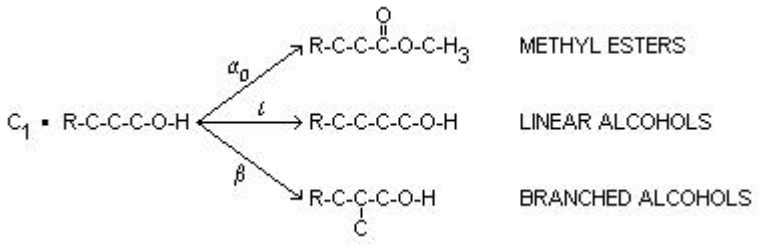


***Figure 4.*** *Dominant mechanisms in higher alcohol synthesis*

Klier et al. [14] have also used Cs-promoted catalysts for higher alcohol synthesis. They used a double-bed reactor packed with $Cs/Cu/ZnO/Cr_2O_3$ and high temperature $Cs/ZnO/Cr_2O_3$ catalysts and sent hydrogen-deficient syngas. Main products obtained were isobutanol and methanol.

They have also tested other catalysts in this dual-bed reactor system. Over $SO_4^{2-}/ZrO_2$ and H-mordenite, a product distribution including butane, methyl-isobutyl ether (MIBE), methyl-tertiarybutyl ether (MTBE) (minor) and dimetyl ether was obtained. Using Amberlyst-15 instead of H-mordenite resulted in an increase in the selectivity of MTBE. MTBE is known to be an octane enhancer; whereas, MIBE is a potential cetane booster.

Ehwald et al. [16] have tested silica supported Rh, Rh-Mn-Li, Rh-Ir-Mn-Li, Rh-Mn-Li-Cu-Zn and Cu-Zn catalysts, and some mixtures of these catalysts for ethanol synthesis. It is known that rhodium catalysts especially when promoted by elements like iron, manganese and molybdenum exhibit high selectivities towards $C_2$-oxygenates. The reasons of those high selectivities can be attributed to the promoter's ability,

- to create new active sites with direct interaction of CO oxygen with the promoter cation,
- to create new active sites for the activation of hydrogen (as in the case of Mo),
- to stabilize positive oxidation states of rhodium by electronic interaction.

Previous studies showed that addition of Fe to $Rh\text{-}Ir/SiO_2$ catalyst helps converting the primary product, acetaldehyde, into ethanol.

Copper catalysts are known to be active for hydrogenation of acetaldehyde to ethanol and for hydrogenolysis of aliphatic acetates to ethanol and their corresponding alcohols. $Rh/SiO_2$ catalyst produces hydrocarbons, methanol, ethanol and acetaldehyde. Addition of Mn and Li (over $Rh\text{-}Mn\text{-}Li/SiO_2$) changes the product distribution as ethanol, acetaldehyde and acetic acid. Therefore, further addition of $CuO\text{-}ZnO\text{-}SiO_2$ as a second component to the promoted Rh catalyst results in an increase in both activity and ethanol selectivity as in the other two-component systems.

Rh-Mn-Li catalyst shows better results in terms of activity when compared to Rh-Ir-Mn-Li catalyst. This is because presence of Ir causes formation of a surface alloy destructing the rhodium ensembles on the surface which are necessary for hydrocarbon formation. On the other hand, Li reduces the hydrogenation ability of the catalyst. Yet, compared to these catalysts, poorer result was obtained with CuO-ZnO catalyst.

Transmission electron micrographs have shown that effects of promoters are not due to a particle size difference. This is because particle sizes do not differ from each other much.

Increase in pressure promoted the selectivities for methanol, ethanol and other oxygenates. Increase in temperature, alternatively, increased methane selectivity.

Rh-Mn-Li-Cu-Zn/$SiO_2$ catalyst was the poorest catalyst among all as Zn was inhibiting the activity of Rh for CO hydrogenation while Cu was decorating the active Rh sites.

## 2.2. Reaction Thermodynamics of Ethanol-Water Systems

The thermodynamic feasibility of ethanol steam reforming has been examined by various studies [17,18,19]. Effects of operational parameters on equilibrium composition can be identified either by stoichiometric thermodynamic approach (STA) or by nonstoichiometric thermodynamic approach (NSTA) [19]. In NSTA, the equilibrium composition of the system is found by direct minimization of the Gibbs free energy for a given set of species without specifying any possible reactions. In STA, on the other hand, the system is described by a set of stoichiometrically independent reactions. Major drawback of STA is that such *arbitrarily* chosen chemical reactions may lead to erroneous results. To eliminate the potential of arriving at such flawed conclusions, Fishtik et al. [19] have introduced the concept of what they call as response reactions (RERs). In their study, they have transformed their arbitrary set of

stoichiometrically independent reactions to be used in STA into response reactions which are unique, and thus, independent of the initial choice of that set of reactions.

Vasudeva et al. [18] used NSTA considering nine species at equilibrium: Ethanol, *acetaldehyde*, methane, carbon monoxide, carbon dioxide, hydrogen, water, *ethylene* and *elemental carbon*. They also carried out calculations considering six of those species excluding the ones written above in an italic fashion to be comparable with the work done by Garcia and Laborde [17]. Results showed that hydrogen formation is favored at high temperatures with low concentrations of water, and at low temperatures with high water concentrations. On the other hand, they have also observed that high water amount in the feed reduces both the carbon monoxide amount and the amount of elemental carbon produced per ethanol. Temperature, however, plays differently, favoring carbon monoxide at high temperatures, and elemental carbon at low temperatures.

Fishtik et al. [19] also made use of NSTA and obtained a distribution of species based on 7 species (ethanol, acetaldehyde, methane, carbon monoxide, carbon dioxide, hydrogen and water) as a function of temperature at 1 atm for an equimolar ethanol:water feed. According to their analysis, methane is the dominant species at low temperatures whereas it is hydrogen at high temperatures. As mentioned above, they have also used STA for their analysis. They have predicted the behavior of the system by selecting a particular limited set of reactions (RERs) whose contribution to the system's response is the most significant. As this is the case, here it should be noted that this analysis is limited to equilibrium systems, and hence, the reactions derived only describes the system's response at equilibrium upon changing the operational parameters.

Fishtik et al. [19] finally concluded that at low water concentrations, ethanol decomposes according to:

$$2\,C_2H_5OH \leftrightarrow 3\,CH_4 + CO_2 \quad \text{and,} \tag{8}$$

$$C_2H_5OH \leftrightarrow CH_4 + CO + H_2 \tag{9}$$

Reaction (8) is dominant at lower temperatures, whereas reaction (9) at higher temperatures. The steam reforming reaction, on the other hand, dominates at 700-800 K and with high water:ethanol ratios which also promotes water-gas shift reaction and methane steam reforming:

$$CO + H_2O \leftrightarrow CO_2 + H_2 \tag{10}$$

$$CH_4 + 2\,H_2O \leftrightarrow CO_2 + 4\,H_2 \tag{11}$$

Ioannides [20] has carried out thermodynamic analysis of hydrogen production from ethanol with respect to solid polymer fuel cell (SPFC, also called as PEM fuel cell) applications. The system consisted of a high-temperature steam reforming or partial oxidation (POX) reactor in which ethanol is converted to a gaseous mixture of $H_2$, CO, $CO_2$ and $CH_4$. This reactor is followed by a low-temperature water-gas shift reactor where CO reacts with $H_2O$ giving $H_2$ and $CO_2$. As this reaction is equilibrium limited, there is the selective CO oxidation reactor coming afterwards to lower CO below 10 ppm levels. Effluent of the selective CO oxidation reactor is sent to solid polymer fuel cell which is integrated to the system in such a way that when a steam reformer is used, the effluent of SPFC (especially, non-converted hydrogen) is recycled back to reformer to obtain higher conversion efficiencies to electrical energy. As a consequence of this, the system will operate under conditions of incomplete fuel utilization. Ioannides has concluded that, for the steam reforming case, employment of feeds with water:ethanol ratios higher than 3 does not offer any significant advantage as this reduces the overall efficiency as a result of recycling due to increased enthalpy needs for water evaporation in the reformer. Even with lower feed ratios, system with POX reactor gave a slightly better maximum hydrogen yield when compared to the maximum of the system with steam reformer. Systems of POX need higher volumetric flow rates as hydrogen

concentration is lowered due to dilution with nitrogen. However, still they are simpler in construction and exhibit faster response characteristics under transient conditions which is necessary especially for vehicle applications.

Tsiakaras and Demin [21] have studied the thermodynamic analysis of a solid oxide fuel cell system (SOFC) fuelled by ethanol. They fed SOFC with the products of ethanol steam reforming, ethanol reforming with $CO_2$ and ethanol partial oxidation with air, being in thermodynamic equilibrium. At $T < 950$ K and $T > 1100$ K products of steam reforming gave the maximum efficiency, and at intermediate temperatures, it was reforming with $CO_2$ leading to maximum. Efficiency obtained by ethanol partial oxidation was, on the other hand, about 20% lower than the maximum.

## 2.3. Steam Reforming

There are many studies dealing with methanol steam reforming in the literature; however, ethanol steam reforming and hydrogen production from ethanol by autothermal reforming are new areas of study. This section will divide into subsections based on the catalysts used in those studies.

### 2.3.1. Studies on Supported Cu Catalysts

Choi and Stenger [22] presented the results of experiments of the methanol decomposition reaction catalyzed by a commercial $Cu/ZnO/Al_2O_3$ catalyst both in the absence and presence of water. Tests were performed under catalyst loading of 0.25 – 1.0 g and GHSV of 1000 – 10000 $h^{-1}$. It was observed that water addition to the feed increased the yield of hydrogen and reduced the formation of by-products like dimethyl ether, methyl formate and methane. However, Choi and Stenger have also concluded that a good methanol synthesis catalyst is not always a good decomposition catalyst especially due to rapid deactivation in the decomposition environment. The causes of this deactivation were listed as copper sintering, carbon decomposition and change of catalyst

structure. For instance, for $Cu/ZnO/Al_2O_3$ catalyst, it has been shown by Cheng [23] that the reduction of ZnO and formation of Cu-Zn alloys cause an initial and rapid decrease of activity for methanol decomposition. In his study, he reported that activity over a Cu/ZnO catalyst is less than that over Cu/Cr/Mn catalyst containing no ZnO.

Choi and Stenger [22] accepted that Cu-O active sites are formed by the dissociative adsorption of water. Therefore, the source of oxygen for the Cu-O site was water in the feed, and copper could be oxidized repeatedly by the following redox mechanism:

$$H_2O + Cu* + 2* \rightarrow 2H* + O - Cu* \quad (12)$$

$$CO + O - Cu* \rightarrow CO_2 + Cu* \quad (13)$$

$$2H* \rightarrow H_2 + 2* \quad (14)$$

A fresh catalyst is largely in the form of oxidized copper after calcination. That is why it should have a higher methanol decomposition rate. If little or no water is fed, the oxidized copper sites reduce to metallic copper which will result in a decrease in activity.

Reddy et al. [24] have reported the synthesis of isobutyraldehyde, which is a very useful chemical feedstock in plastics industry, from methanol and ethanol in a single step over $CuO/ZnO/Al_2O_3$ catalyst. They used ethanol and methanol as the reactants and obtained the following product distribution: Isobutyraldehyde, acetaldehyde, formaldehyde, higher hydrocarbons, acrolein and $CO_x$. Isobutyraldehyde production increased in the presence of following species: Air < air + $H_2O$ < $N_2$ < $N_2$ + $H_2O$. $CuO/Al_2O_3$ is a ethanol dehydrogenation catalyst and the basic nature of ZnO promotes this ability. Ethanol is first converted into acetaldehyde which reacts with methanol to produce isobutyraldehyde over $CuO/ZnO/Al_2O_3$.

Catalyst coking and production of by-products like methane, acetaldehyde and diethyl ether, arise as the major problems faced in the studies of ethanol steam reforming. Formation of ethylene during steam reforming leads to catalyst coking [26]. Starting from this, Freni et al. [25] have proposed a two-layer fixed-bed catalytic reactor for ethanol steam reforming reaction. They first converted ethanol into acetaldehyde over $Cu/SiO_2$ catalyst under low temperature, and then converted acetaldehyde into syngas over Ni/MgO catalyst. They carried out the tests with a total gas flow rate of 218 $cm^3$/min at GHSV of 109000 $h^{-1}$, and using a feed of 8.2:1 water to ethanol ratio. Individual runs either with $Cu/SiO_2$ or with Ni/MgO catalyst only were also performed. The former one resulted in the formation of only acetaldehyde and hydrogen with 100% ethanol conversion up to 500°C. Above this temperature, ethylene formation and catalyst coking, and hence, catalyst deactivation were observed. The latter one, on the other hand, showed a low coking resistance, yet gave high acetaldehyde selectivity. Conversely, the two-layer system produced a species distribution consisting of only hydrogen, carbon dioxide and carbon monoxide (and traces of methane and acetaldehyde) with 100% of ethanol being converted. Match of the exit compositions with the compositions obtained by a simple equilibrium calculation revealed that the following reactions dominate in the overall and reach equilibrium under operating conditions:

$$C_2H_5OH + H_2O \leftrightarrow 2CO + 4H_2 \quad (15)$$

$$CO + H_2O \leftrightarrow H_2 + CO_2 \quad (16)$$

$$CO + 3H_2 \leftrightarrow CH_4 + H_2O \quad (17)$$

Mariño et al. [27] examined the effect of copper loading and calcination temperature on the structure and performance of Cu-Ni-K/γ-$Al_2O_3$ catalyst. Copper size increases with copper loading and calcination temperature. At low Cu loading and low calcination temperatures low Cu size was obtained which gave high dispersion values. Although also affected by the nature of the active sites, high TOF values were obtained under high dispersions. Thus, they

concluded that ethanol steam reforming reaction is in fact a structure sensitive reaction. Apart from the structure of the catalyst, Cu is an active agent, and Ni promotes C-C bond rupture and increases hydrogen selectivity, and potassium neutralizes the acidic sites of γ alumina which improves the performance of the catalyst.

The above discussion was argued lately again by Mariño et al. [28]. They have re-stated the followings: Metallic copper produces a fast ethanol dehydrogenation to acetaldehyde. Nickel favors the C-C bond rupture of acetaldehyde to produce methane and carbon monoxide. Potassium, on the other hand, prevents dehydration reaction to form ethylene or diethylether by neutralizing the acidic sites of the support.

They further reported that increase in the calcination temperature results in a strong interaction between nickel and aluminum which decreases reducibility of nickel, and along with this, decreases the selectivity towards $C_1$ compounds. This is in agreement with what had been proposed by Mariño et al. earlier [27].

### 2.3.2. Studies on Supported Group VIIIB Metal Catalysts

Galvita et al. [29] have used the two-layer fixed-bed catalytic reactor of their previous study (§2.3.1) [25] to test, this time, a palladium-based catalyst and again a nickel-based catalyst in a similar manner. They carried out the experiments by supplying water-ethanol solutions of 8.1:1 and 1.04:1 mol ratios as feed and at WHSV of 1600-2200 $cm^3$/h-g catalyst. Again, first of all, they tested the catalysts individually. Over Pd catalyst supported on Sibunit[2] only hydrogen, methane, carbon monoxide and carbon dioxide were produced in a range of 210-380°C. It was shown that the following two reactions were taking place:

[2] A special porous carbonaceous material.

$$C_2H_5OH \leftrightarrow CH_4 + CO + H_2 \quad (18)$$

$$CO + H_2O \leftrightarrow CO_2 + H_2 \quad (19)$$

As water amount in the feed decreased, water-gas shift reaction became less important as it can easily be deduced from Le Châtelier's principle. This shifts the minimum temperature at which 100% ethanol conversion is attainable (330°C) to a slightly higher value (360°C). On the other hand, over the industrial Ni-containing GIAP-16 catalyst, acetaldehyde, methane, hydrogen and carbon oxides were produced. Substantial amounts of coke were also observed.

Alternatively, in the two-layer system, hydrogen, carbon oxides and methane were detected as the products with methane in trace amounts. Temperature of the Pd layer was kept at 335°C, and that of Ni layer was varied between 650 and 800°C. Methane steam reforming reaction took place along with Reaction (18) and Reaction (19) in the overall, all being in equilibrium:

$$CH_4 + H_2O \leftrightarrow CO + 3H_2 \quad (20)$$

In a later study of Galvita et al. [30] characteristics of the Pd catalyst and its catalytic performance in ethanol decomposition in steam were discussed in more detail. TEM micrographs and XP spectra of both fresh and sent catalysts showed no difference. In order to identify the intermediate species, the mechanism of the overall reaction taking place, and the fast and slow steps in the reaction pathway, WHSV was increased from 2200 to 33000 $cm^3$/h-g catalyst. At the end the following mechanism was proposed:

$$C_2H_5OH \leftrightarrow CH_3CHO + H_2 \quad (slowest) \quad (21)$$

$$CH_3CHO \rightarrow CH_4 + CO \quad (fast) \quad (22)$$

$$CO + H_2O \leftrightarrow CO_2 + H_2 \quad (slow) \quad (23)$$

Freni [31] has tested $Rh/Al_2O_3$ catalyst and the alumina support for ethanol steam reforming reaction for molten carbonate fuel cell applications. He showed that alumina results in dehydration of ethanol forming ethylene and water at temperatures higher than 600 K for a feed consisting 90% water. He further showed that water content of the feed does not influence the ethylene formation. $Rh/Al_2O_3$ catalyst, on the other hand, produced carbon monoxide and methane below 730 K (with ethanol dehydrogenation into ethoxide as the intermediate step), and above this temperature ethanol steam reforming prevailed with 100% ethanol conversion and no yield of $C_2H_4$ or $CH_3CHO$. The time-on-stream data showed no selectivity changes; however, ethanol conversion decreased with time. This is attributed to the loss of the catalyst dispersion degree as a result of a size modification of the catalyst particles under thermal effect of the reaction temperature which caused catalyst grains to grow.

Fatsikostas et al. [32] presented the results of the experiments done on $Ni/La_2O_3$, and reported that this catalyst shows high activity, high hydrogen selectivity, as well as good long term stability. They conducted the tests in a temperature range of 300-800°C sending a feed of 3:1 water-ethanol ratio at a space time (W/F) range of 0.01 to 0.23 g catalyst.s/cm$^3$. Tests carried out at very high space time (0.0375 g catalyst.s/cm$^3$) showed that ethanol steam reforming takes place to a significant extent above 400°C. 100% ethanol conversion was achieved only at about 700°C. Furthermore, it is the ethanol dehydrogenation that is the dominant reaction at low temperatures which becomes less important above 500°C as acetaldehyde begins to reform. As $La_2O_3$ does not have an acidic nature no ethylene is produced. At high temperatures the only reaction products were carbon monoxide and hydrogen, with carbon dioxide (from water-gas shift reaction) and methane (from methanation reaction[3]) as being the by-products. Tests on different space velocities also revealed that at contact times higher than 0.1 g catalyst.s/cm$^3$ (at 750°C) it is possible to achieve 100% ethanol conversion and hydrogen selectivities higher than 95%. Time-on-stream data, on the other

[3] $2CO + 2H_2 \leftrightarrow CH_4 + CO_2$

hand, proved the stability of the catalyst only with a little deactivation as a result of decrease in ethanol conversion, although no significant change in hydrogen selectivity was observed.

***Table 2.*** *Effects of process parameters in the study of Liguras et al. [33]*

| **Parameters** | **Effect on/of** | **Observation** |
|---|---|---|
| Metallic Phase<br>1% *Me*/γ-$Al_2O_3$ | $X_{C2H5OH}$ | Rh >> Pt > Pd > Ru |
| | $S_{H2}$, $S_{CO}$ | Rh >> Pt > Ru = Pd |
| | $S_{CO2}$ | All but especially Pt, Rh |
| | $S_{CH3CHO}$, $S_{C2H4}$ | All but especially Rh |
| | $S_{CH4}$ | None. Rh, a little |
| Metal Loading<br>*0.5-2%* Rh/γ-$Al_2O_3$<br>*1-5%* Ru/γ-$Al_2O_3$ | Increase in Rh amount | $T_{100\%\ conv}$, $S_{H2}$, $S_{CO2}\uparrow$<br>$S_{CO} \rightarrow$<br>$S_{byprod} \downarrow$ |
| | Increase in Ru amount | $S_{H2}$, $S_{CO2}$, $S_{CO}\uparrow$<br>$T_{100\%\ conv}$, $S_{byprod} \downarrow$ |
| 5% Ru/*Support* | $X_{C2H5OH}$, $S_{prod}$, $S_{byprod}$ | $Al_2O_3$ > MgO > $TiO_2$ |
| Space velocity (W/F) *0.018-0.105 g catalyst.s/cm$^3$* | Increase in W/F | $X_{C2H5OH}$, $S_{H2}$, $S_{CO}\uparrow$<br>$S_{CO2}$, $S_{byprod}\downarrow$ |

Liguras et al. [33] have investigated the effect of Rh, Ru, Pt and Pd catalysts supported on $Al_2O_3$, MgO and $TiO_2$ and the effect of metal loading on the catalytic performance towards ethanol steam reforming. They performed the experiments feeding ethanol and water in stoichiometric ratios with respect to ethanol steam reforming reaction giving $CO_2$. They worked under W/F range of

0.018 to 0.105 g catalyst.s/cm$^3$, and at a temperature range of 600-850°C. Complete conversion was obtained at 800°C under severe conditions over 1% $Rh/Al_2O_3$ catalyst. Acetaldehyde, ethylene (over acidic alumina) and methane (from hydrogenation of carbon oxides) were formed as by-products, yet with low selectivities. At temperatures near 800°C, selectivity of ethylene decreased to zero (as that of acetaldehyde) due to steam reforming of ethylene. Effects of all process parameters are summarized in Table 2 for this study. Finally, long-term stability test was also carried out for 5% $Ru/Al_2O_3$ catalyst and the results were similar to what has been reported by previous studies [31,32]: No change in hydrogen selectivity (and selectivity to methane, acetaldehyde and ethylene), decrease in ethanol conversion.

Cavallaro et al. [34] also studied the ethanol steam reforming on $Rh/Al_2O_3$ catalyst, and investigated the influence of reaction temperature (550-650°C), water:ethanol ratio (4.4-12.4), space velocity (5000-30000 h$^{-1}$) and oxygen in the reacting medium. Results of the experiments showed that high temperatures and low space velocities are necessary to optimize hydrogen production. Runs performed at different GHSV values revealed that ethanol first dehydrogenates into acetaldehyde which either decomposes into methane or reforms with steam into hydrogen. Methane further undergoes steam reforming. Steam reforming of methane occurs with a lower rate respect to water-gas shift reaction. On the other hand, acetaldehyde decomposition is faster compared to ethanol dehydrogenation. Furthermore, catalyst deactivation caused by metal sintering and coke formation was registered. Addition of oxygen, alternatively, promoted not only metal sintering as a result of hot spot phenomena but also the ethanol conversion through oxidative dehydrogenation:

$$C_2H_5OH + \tfrac{1}{2}O_2 \leftrightarrow CH_3CHO + H_2O \qquad (24)$$

Deluga et al. [7] have also studied hydrogen production from ethanol and ethanol-water mixtures over rhodium catalyst, however, supported on ceria.

Alternatively they have studied autothermal reforming, and obtained 100% hydrogen selectivity with more than 95% ethanol conversion under as high a space velocity as 360000 $h^{-1}$, and even under higher velocities than this one. They carried out the runs at 140°C. Yet the catalyst temperature reached about 700°C as oxidation reaction was also taking place. They have also performed a simple economic analysis considering an ethanol cycle starting from photosynthesis and ending in a perfect fuel cell. They concluded that under such a hypothetic, completely reversible, ideal system the fuel cost (cost of ethanol to generate electricity) would be about $0.04 per kWh. They finally suggested that it may be possible to capture more than 50% of the energy from photosynthesis as electricity.

Llorca et al. [35] have studied the effect of supports of cobalt catalysts on ethanol steam reforming under a mixture of 1:13:70 ethanol:water:argon (molar ratio) in a temperature range of 300-450°C and at 5000 $h^{-1}$ GHSV. Supports tested are the following: MgO, γ-$Al_2O_3$, $SiO_2$, $TiO_2$, $V_2O_5$, ZnO, $La_2O_3$, $CeO_2$ and $Sm_2O_3$. Ethanol steam reforming occurred to a large extent over ZnO-, $La_2O_3$-, $Sm_2O_3$-, and $CeO_2$-supported catalysts. Different GHSV values and/or different Ar to ethanol and water ratios were also studied over Co/ZnO catalyst which showed the best result in terms of 74% hydrogen selectivity under 100% ethanol conversion. These experiments revealed that as GHSV increases decomposition of ethanol to acetone decreases while the extent of the steam reforming reaction increases. Further increase of GHSV increased the selectivity to acetaldehyde which proved ethanol dehydration to be an intermediate step in ethanol steam reforming.

### 2.3.3. Comparative Studies

This subsection includes studies comparing Group VIIIB metal catalysts both among each other and with other catalysts, and different oxide catalysts.

Cavallaro and Freni [36] tested several catalysts for ethanol steam reforming to be used indirectly in molten carbonate fuel cells (MCFCs). As the operating temperature of MCFC is above 900 K, the results of the experiments carried out at atmospheric pressure were extrapolated to temperatures 800-900 K and pressures up to 100 bar by using a mathematical model. Experiments done at high temperatures (630-750 K) showed no trace of intermediate oxidation products like acetaldehyde, acetic acid or ethyl acetate the production of which are more important on copper catalysts. For temperatures lower than 600 K, however, the selectivity to carbon dioxide and hydrogen decreases due to higher oxygenate formation. It was observed that acetic acid selectivity is directly related to the water:ethanol ratio, whereas ethyl acetate selectivity seems to be related to conversion and temperature. Runs with different space velocities revealed that acetaldehyde is produced as the first step which is followed by an oxidative step to ester (under slightly excess water) or to acetic acid (under excess water). All catalysts tested shifted the system towards equilibrium above 630 K. $CuO/ZnO/Al_2O_3$ and $NiO/CuO/SiO_2$ catalysts do not produce coke and/or oxygenated side-products even with water:ethanol ratio lower than 3 although some catalysts require ratios higher than 4. Noble metal (Pt, Rh) and W-based catalysts showed almost the same activity as $CuO/ZnO/Al_2O_3$. Finally, mathematical model showed that it is possible to obtain good hydrogen yields of 30-50% even at high pressures (which thermodynamically reduce hydrogen selectivity) in MCFC separated from the reformer side by a membrane.

Takezawa and Iwasa [37] argue that the differences in catalytic performances of copper and Group VIIIB metals in methanol steam reforming and methanol dehydrogenation are due to the differences in the reactivity of HCHO intermediate involved. In the beginning of their study, they summarize all information available in the previous studies on copper and Group VIIIB metal catalysts. Firstly, over copper and Pd/ZnO catalysts, methanol dehydrogenates into acetic acid; whereas over other Group VIIIB metals syngas is formed from methanol as shown below, respectively:

***Table 3.*** *Mechanisms and products in the study of Takezawa and Iwasa [37]*

| Feed | Catalyst | Reaction Mechanisms and/or Product Distributions |
|---|---|---|
| $CH_3CHO$/ $H_2O$ | VIIIB metal/$SiO_2$ | Methanol decomposition (main)<br>$CH_3OH \rightarrow CO + 2H_2$<br>Steam Reforming<br>$CH_3OH \rightarrow CO + 2H_2 \xrightarrow{H_2O} CO_2 + H_2$ |
| | Cu, Cu/$SiO_2$ | Steam Reforming<br>$CH_3OH \xrightarrow{-H_2} HCHO \xrightarrow{H_2O\,(or\ HO-)} HCOOH\,(or\ HCOO-) \rightarrow CO_2 + H_2$ |
| $HCHO$/ $CH_3OH$ | Cu, Cu/$SiO_2$ | Acetic acid formation<br>$CH_3OH \rightarrow HCHO \xrightarrow{CH_3OH\,(or\ CH_3OH-)} HCOOCH_3$ |
| | Pt/$SiO_2$, Pd/$SiO_2$ | Formaldehyde decomposition (main)<br>$HCHO \rightarrow CO + H_2$<br>Methanol decomposition<br>$CH_3OH \rightarrow CO + 2H_2$ |
| $C_2H_5OH$/ $H_2O$ | Cu/$SiO_2$ | Products: $CH_3COOH$ (main), $CH_3CHO$, $H_2$, $C_4$-species |
| $CH_3CHO$/ $H_2O$ | Cu/$SiO_2$ | Products: $CH_3COOH$, $H_2$<br>(Also: Butyraldehyde, ethanol)<br>Steam reforming of acetaldehyde (main)<br>$CH_3CHO + H_2O \rightarrow CH_3COOH + H_2$<br>Hydrogenation of acetaldehyde<br>$CH_3CHO + H_2 \rightarrow C_2H_5OH$ |
| $C_2H_5OH$ | Pd, Pt, Ni | Products: $CH_4$, CO, $H_2$, $CH_3CHO$<br>Dehydrogenation of ethanol<br>$C_2H_5OH \rightarrow CH_3CHO + H_2$<br>Decomposition of acetaldehyde<br>$CH_3CHO \rightarrow CH_4 + CO$ |

- $2CH_3OH \leftrightarrow HCOOCH_3 + 2H_2$ (25)
- $CH_3OH \leftrightarrow CO + 2H_2$ (26)

On the other hand, copper and Pd/ZnO catalysts hydrogenate unsaturated aldehydes/ketones to unsaturated alcohols while other Group VIIIB metal catalysts to saturated aldehydes/ketones. Also, hydrogenation of esters and carboxylic acids to alcohols which is dominant over Pd/ZnO catalyst occurs more over Cu catalysts when compared to other Group VIIIB metal catalysts.

In this study, Takezawa and Iwasa further tested Cu, Ni, Rh, Pd and Pt catalysts supported on various oxides (MgO, $La_2O_3$, $Nd_2O_3$, $MnO_2$, $Cr_2O_3$, $HfO_2$, $Na_2O_5$, $Al_2O_3$, $SiO_2$, ZnO) feeding different mixtures to the reactor to understand the reaction mechanisms taking place. Reactions taken place and product distributions obtained are summarized in Table 3 for various mixtures fed to the system.

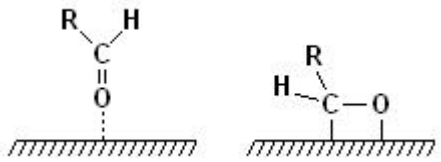


***Figure 5.*** *Adsorption of aldehydes on IB (left) and VIIIB metals [37]*

It was re-stated in the study that adsorption of aldehydes on IB and VIIIB metals occur differently as shown in Figure 5 which is the basic reason of the difference in the reactivity of formaldehyde intermediate, HCHO, and hence, the product distributions obtained as indicated in Table 3.

As mentioned above, catalytic activity of Pd/ZnO catalyst is similar to that of copper catalysts. This is because formaldehyde adsorbs on positively charged Pd sites of the PdZn alloy formed. On the other hand, the highest selectivity for steam reforming was obtained over Pd catalysts which increased with increase in temperature. Best performance was obtained at 30wt% Pd loading.

In a later study, Iwasa et al. [38] have produced acetaldehyde at low conversion levels and at high space times over Pd-Zn, Pd-Ga and Pd-In alloys of Pd catalysts as also produced over Cu/ZnO catalyst. At higher temperatures and lower space times, formation of ethyl acetate was observed with some decrease in acetaldehyde selectivity suggesting that ethyl acetate was produced through acetaldehyde. Over metallic Pd, however, decomposition of ethanol to CO and $CH_4$ took place. Iwasa et al. have also pointed out the effects of different catalyst preparation methods on activity tests of the same catalyst.

Aupretre et al. [4] investigated the nature of metals and oxides to maximize hydrogen production while minimizing carbon monoxide formation. They used a feed of (12.8 vol% ethanol + 38.4% water + 48.8% $N_2$) to reach a total flow rate of 100 $cm^3$/min. They carried out the experiments at 500-800°C. They proposed a mechanism such that ethanol is to be activated on the metal and water on the support. Based on this mechanism, Rh, Pt, Pd, Ru, Ni, Cu, Zn and Fe were tested along with $Al_2O_3$, $CeO_2$-$Al_2O_3$, $CeO_2$, $CeO_2$-$ZrO_2$ and $ZrO_2$ as the oxide supports. Results of the experiments showed that carbon dioxide is produced in ethanol steam reforming; therefore, metals to be used in active and selective catalysts for ethanol steam reforming should be highly active in steam reforming, and poorly efficient in water-gas shift reaction. To improve performances of the catalyst in steam reforming ceria-containing supports were used which enable enhanced OH surface mobility, and promote water-gas shift reaction. Rh and Ni catalysts are active for steam reforming and not for water-gas shift reaction. Table 4 summarizes the results obtained over those catalysts. As a final note, Pt, Cu, Zn and Fe catalysts supported on $\gamma$-$Al_2O_3$ was highly

***Table 4.*** *Effect of supports on $H_2$ yield and $CO_2$ selectivity in the study of Aupretre et al. [4]*

| Parameter | Effect on | Observation |
|---|---|---|
| 1% Rh/*Support* | $H_2$ yield | $Ce_{0.63}Zr_{0.37}O_2$ > 12%$CeO_2$-γ-$Al_2O_3$ > $CeO_2$ > γ-$Al_2O_3$ |
| | $CO_2$ Selectivity | γ-$Al_2O_3$ > 12%$CeO_2$-γ-$Al_2O_3$ > $CeO_2$ > $Ce_{0.63}Zr_{0.37}O_2$ |
| 9.7% Ni/*Support* | $H_2$ yield | $Ce_{0.63}Zr_{0.37}O_2$ > $CeO_2$ > 12%$CeO_2$-γ-$Al_2O_3$ > γ-$Al_2O_3$ |
| | $CO_2$ Selectivity | γ-$Al_2O_3$ > 12%$CeO_2$-γ-$Al_2O_3$ > $CeO_2$ > $Ce_{0.63}Zr_{0.37}O_2$ |

***Table 5.*** *Summary of the results of the study by Llorca et al. [39]*

| Oxide | Nature of active site | Observation |
|---|---|---|
| $SiO_2$ | - | No conversion |
| MgO | Basic | High acetaldehyde selectivity, negligible steam reforming |
| γ-$Al_2O_3$ | Acidic | Ethylene as the only product |
| $V_2O_5$ | Acidic | Ethylene as the major product |
| $La_2O_3$ | Basic | Ethylene as the major product |
| $Sm_2O_3$ | Basic | Ethylene as the major product |
| ZnO | Basic, redox property | Ethanol decomposes to acetone and acetaldehyde over basic sites. Redox characteristics help acetaldehyde to convert into hydrogen. |

active for water-gas shift reaction although they showed moderate activity for steam reforming.

Llorca et al. [39] tested various oxides for steam reforming reaction at 300-450°C. Results of this study are listed in Table 5. Best performance was obtained by ZnO which gave highly effective production of CO-free hydrogen with 100% ethanol conversion.

# CHAPTER 3

# EXPERIMENTAL AND METHODOLOGY

In this study, $ZnO/SiO_2$ catalysts with different copper and palladium loadings, and Co doped SBA-15 catalyst were prepared by different sol-gel techniques, characterized to some extent by Thermal Gravimetric Analysis (TGA), and Brunauer-Emmett-Teller (BET) techniques, and tested for their activity and selectivity in ethanol steam reforming in a packed-bed reactor.

## 3.1. Catalysts Tested

Catalysts used in this study are listed in Table 6 along with their compositions in weight percents. Set I catalysts comprise promoted and/or supported zinc oxide catalysts, and Set II catalyst is the SBA-15-supported cobalt catalyst. Samples 4,

***Table 6.*** *Compositions of the catalysts tested*

| | **Sample No.** | **Compositions** |
|---|---|---|
| Set I | 1 | 6%Cu/50%ZnO/$SiO_2$ |
| | 2 | 4%Cu/50%ZnO/$SiO_2$ |
| | 3 | 2%Pd/50%ZnO/$SiO_2$ |
| | 4 | 50%ZnO/$SiO_2$ |
| | 5 | 50%ZnO/$SiO_2$ |
| | 6 | 50%ZnO/$SiO_2$ |
| Set II | 7 | 40%Co/SBA-15 |

5 and 6 differ from each other by different water amounts used during preparation.

Set I catalysts were prepared at Izmir Institute of Technology and Set II catalyst was prepared in the Department of Chemistry at METU. Further information on the preparation and characterization of these catalysts is given in Appendices B and C.

## 3.2. Experimental Setup and Activity Measurements

Systems of liquids and gases can become much more complicated, and hence, challenging than it can ever be imagined. A huge portion of this study was spent on establishing a proper experimental setup and especially on finding an answer to how to feed the liquid to the system. After many systems designed, many unsuccessful experiments performed, and many modifications made the setup shown in Figure 6 was put into operation. Below is an explanation on the experimental setup and how activity measurements are carried out.

Ethanol and water mixtures are prepared in ratios according to the stoichiometry of the steam reforming of ethanol to carbon dioxide and hydrogen: 25 mol% (46 wt%) ethanol. The liquid mixture is then injected into a cooler of 25 $cm^3$ kept at 3°C to minimize vaporization effects as the level decreases in the cooler during experiments. A peristaltic pump is used to feed this liquid to the system shown in Figure 6 at an average flow rate of 0.047 $cm^3$/min. The liquid is firstly sent to a bulb of 250 $cm^3$ kept at 160°C by means of heating tapes. Collected in the bulb the vaporized liquids are then directed to the inlet of the reactor and carried into the reactor under a nitrogen and argon flow of 45 $cm^3$/min and ca. 4 $cm^3$/min, respectively, as shown in the enlarged view in Figure 6.

A packed-bed reactor having an inner diameter of 3.8 mm is used for reactivity tests. 0.1 g catalyst is used in each experiment, and the catalyst bed is supported

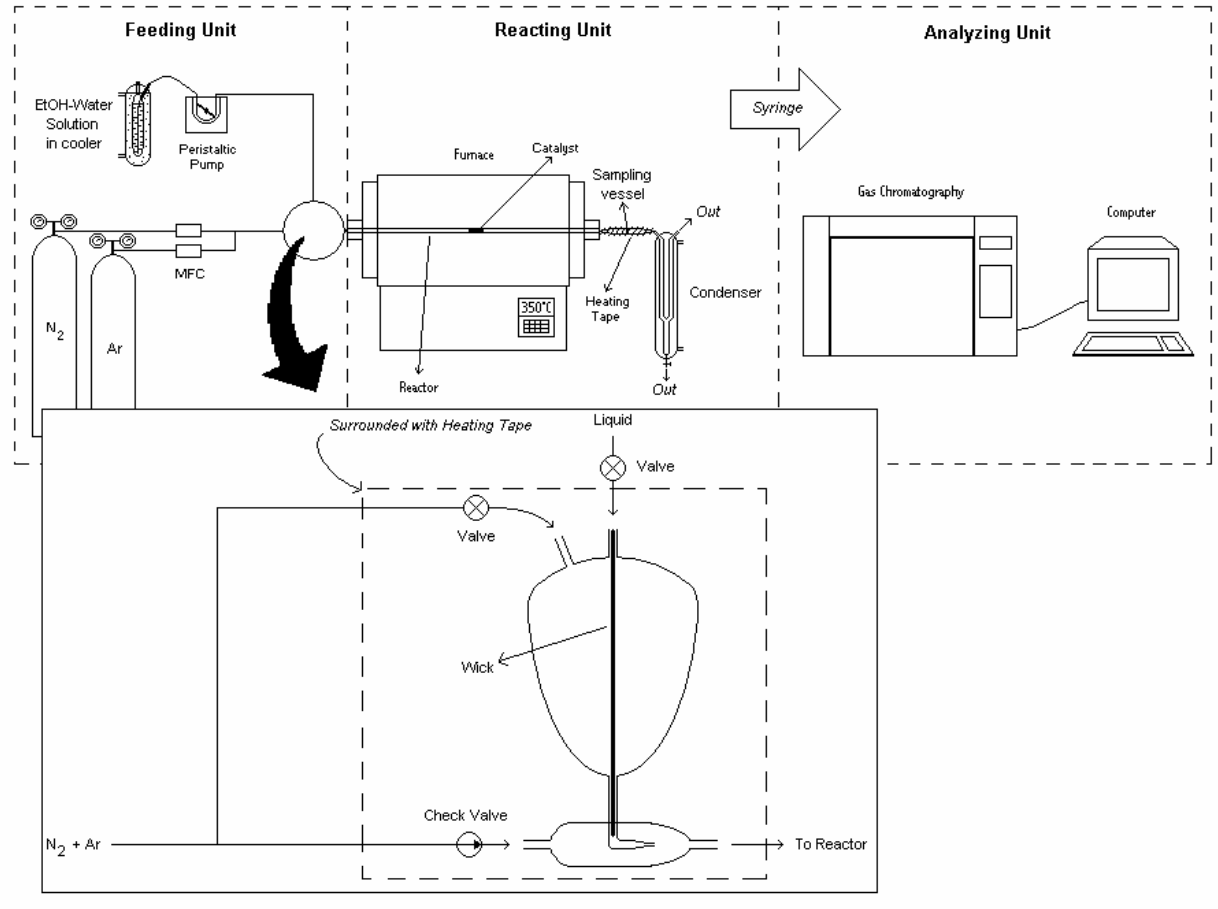


***Figure 6.*** *Experimental Setup*

by quartz wool at both ends. A tubular furnace is used to keep the temperature of the reactor constant at desired values.

Product stream exiting the reactor then flow into a "sampling vessel" which is also heated by heating tapes and kept at 175°C. Sampling vessel has an opening, other than its two ends, which is closed by a septum. Samples are taken into heated gas syringes through this septum to be analyzed. Species which are in liquid phase under room temperature were condensed next in a condenser kept at 3°C. Gaseous species are discharged into atmosphere through fume hoods while liquefied species are collected in bottles for proper disposal.

Analyses were carried out in a gas chromatograph (GC) (HP 4890A) equipped with a Thermal Conductivity Detector (TCD) which uses nitrogen as reference gas. Species are separated in a GasChrom MP-1 packed column (30 ft). Table 7 lists the values of GC settings used during analyses. A long column, low flow rates and a temperature ramp in the oven are necessary for such a system containing components like hydrogen which rapidly adsorbs and desorbs in every column, and components like ethanol which is just the opposite. For this reason, analysis of one sample takes about 1 hour.

***Table 7.*** *GC settings*

| **GC Settings** | **Values** |
|---|---|
| Injection port temperature | 220°C |
| Oven temperature | 75°C (9 min) [4°C/min] 200°C (9.5 min) |
| Detector temperature | 250°C |
| Reference flow | 9-10 $cm^3$/min |
| Column flow | 13-15.5 $cm^3$/min |

Single-point GC calibration was carried out for each species in most of the experiments. For the others, previous calibration data were processed to obtain a collective representative calibration data as explained in detail in Appendix E.

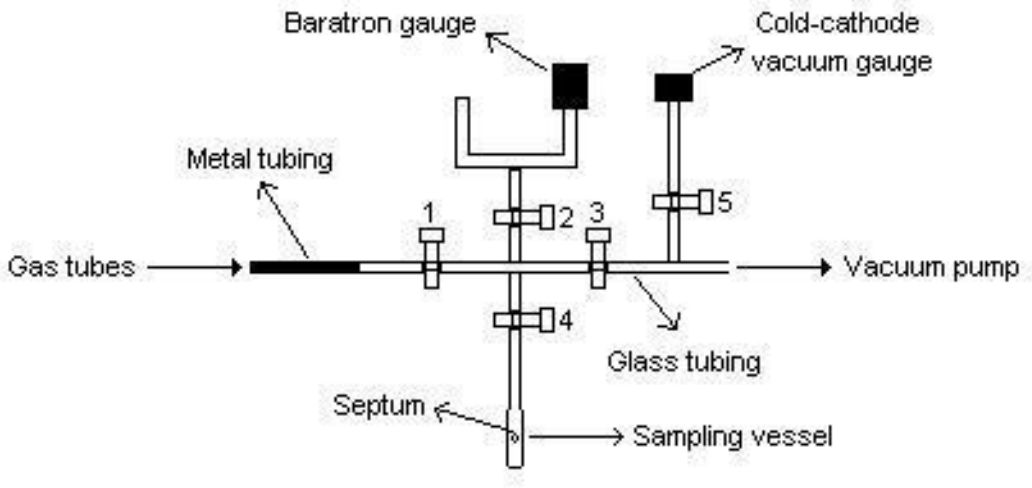


***Figure 7.*** *Manifold used for GC calibration*

Figure 7 shows the manifold used for GC gas calibration. Manifold is firstly vacuumed by a vacuum pump. After closing valve 3, a single gas or a calibration gas[4] with known compositions is sent to the system. The gas is then collected at room temperature and atmospheric pressure in the space obtained by closing valves 1 and 3. The pressure of this gas, and hence, its amount are controlled by a read-out connected to the Baratron gauge. A certain volume is taken into a gas syringe and injected to GC to obtain a mol-to-area relation. On the other hand, liquid calibration is done by using microliter liquid syringes, and a known volume of sample is again injected to GC to get the mol-to-area relation.

[4] Containing carbon monoxide, methane, carbon dioxide and ethylene.

Experiments are carried out at temperatures between 300 and 500°C at intervals of 50°C. Before each experiment the system is heated up under the flow of nitrogen and argon. As the system reaches thermal equilibrium, liquid starts to be fed at which point the valve in the liquid line is opened and the valve in the gas line is closed (Figure 6). Previous experiments showed that no reaction takes place below 300°C. As this is the case, one additional set is performed also at either 200 or 250°C to obtain ethanol and water amounts sent to the system in gaseous phase. Although these values could as well be obtained from liquid pumping flow rate (as already done), as will be discussed in the following chapter, most of the time those values do not come out to be *near*. Some experiments were carried out starting from 200 or 250°C, and by increasing the reactor temperature to 300°C, and then to 350°C and so on. As heating of the furnace is rather rapid compared to its cooling additional time is allowed for the system to re-establish steady state at each temperature. Some experiments, on the other hand, were done starting at 500°C and by letting the furnace cool down which is already a time-consuming process, and the system remains in steady state at each cooling step so no additional time is waited. A sample time schedule of one full experiment is given in Appendix F. At each set, or reactor temperature; one, two or three samples are taken and analyzed in GC sequentially. Before each injection, syringe is heated by a heating gun, and after each injection, syringe is cleaned by a syringe cleaning equipment as shown in Figure 8. Other pictures of the setup are given in Appendix G.

As the total flow rate of the "heated" gaseous mixture at the reactor exit is to be known to do the necessary calculations, which cannot easily be measured by means like soap bubble flow meter, the flow rate is calculated indirectly from a known constant flow rate of a known inert gas component also sent to the system. Nitrogen, the carrier, could have been used for such a purpose; however, it would be impossible to obtain a nitrogen peak in the chromatogram as the reference gas to the GC is already nitrogen. So, argon was used and sent with nitrogen to the system as mentioned above. Use of argon alone both as the

carrier and the *internal standard* would also be of no use as the GC column would saturate with argon which would result in a faulty argon area.


***Figure 8.*** *Heating gun (left) and syringe cleaning equipment*

Few experiments were conducted also under air flow to realize some ethanol oxidation along with ethanol steam reforming, or in other words autothermal reaction. Argon could not be used in these experiments as oxygen in air could not be separated from argon in the column. So, no calibration was done in these experiments as the total flow rate was not known, and instead, the collective calibration data were used to carry out the calculations. Table 8 summarizes the

***Table 8.*** *Flow rates and compositions of liquid and gaseous phases*

| | Unit | [5] | Total | Ethanol | Water | Nitrogen | Oxygen |
|---|---|---|---|---|---|---|---|
| **Liquid phase** | $cm^3/min$ | | 0.047 | 0.012 | 0.035 | - | - |
| | g/min | | 0.043 | 0.020 | 0.023 | - | - |
| | mol/min | | 0.0017 | 0.00044 | 0.0013 | - | - |
| | mol% or vol% | | 100 | 25 | 75 | - | - |
| | wt% | | 100 | 46 | 54 | - | - |
| **Gaseous phase** | $cm^3/min$ | S | 86 | 10 | 31 | 45 | 0 |
| | | H | 86 | 10 | 31 | 36 | 9.4 |
| | | L | 51 | 10 | 31 | 0 | 9.4 |
| | g/min | S | 0.096 | 0.020 | 0.023 | 0.053 | 0 |
| | | H | 0.091 | 0.020 | 0.023 | 0.042 | 0.0064 |
| | | L | 0.049 | 0.020 | 0.023 | 0 | 0.0064 |
| | mol/min | S | 0.0036 | 0.00044 | 0.0013 | 0.0019 | 0 |
| | | H | 0.0037 | 0.00044 | 0.00131 | 0.0015 | 0.00040 |
| | | L | 0.0021 | 0.00044 | 0.0013 | 0 | 0.00040 |
| | mol% or vol% | S | 100 | 12 | 36 | 52 | 0 |
| | | H | 100 | 12 | 36 | 41 | 11 |
| | | L | 100 | 20 | 61 | 0 | 19 |
| | wt% | S | 100 | 21 | 24 | 55 | 0 |
| | | H | 100 | 22 | 25 | 46 | 7.0 |
| | | L | 100 | 40 | 47 | 0 | 13 |

[5] Steam reforming: S. Autothermal reforming: H (High space velocity), L (Low space velocity)

compositions and flow rates of both the liquid phase and the gaseous phase applied in experiments.

Parameters changed in experiments include catalysts, temperature and space velocity. Following chapter presents the results of these tests along with comments and discussions.

# CHAPTER 4

# RESULTS AND DISCUSSION

## 4.1. Characterization Results

BET results of both Set I and Set II catalysts (except Sample 5) are shown in Table 9. For Set I catalysts, as seen in the table, as the amount of metal used in the catalyst increases, BET surface area decreases while average pore diameter also increases.

Cannas et al. [40] have also come up with a similar situation. They observed crystallite phases in XRD patterns and a decrease in BET surface areas as they impregnated more ZnO on silica. They attributed this to the involvement of larger areas of support as the dispersing phase (ZnO) is in higher amount. This way, the dispersing phase is spread over the surface in a homogeneous way. Increase in the amount of metal used in the catalysts may have resulted in formation of larger and denser silica suspensions which end up with having such BET areas as explained by Cannas et al. [40].

Cannas et al. also presented the results of XRD patterns of their $ZnO/SiO_2$ catalysts as the calcination temperature increases. According to their data, ZnO zincite phases were observed in catalysts calcined at temperatures between 500 and 700°C. So, it is very likely to have zincite phases in our catalysts. Above 800°C, however, a solid state reaction between zinc oxide and the silica matrix was detected by Cannas et al. which resulted in the formation of zinc silicates like $\beta$-$Zn_2SiO_4$. Such zinc silicate formations might have also occurred as a result of a probable catalytic effect of palladium and/or copper to lower the

necessary reaction temperature from 800°C to our calcination temperature, 500°C.

***Table 9.*** *BET results*

| Catalyst | | | BET Surface Area ($m^2/g$) | BJH Desorption Average Pore Diameter (nm) |
|---|---|---|---|---|
| Set I | 1 | 6%Cu/50%ZnO/$SiO_2$ | 94 | 7.7 |
| | 2 | 4%Cu/50%ZnO/$SiO_2$ | 144 | 7.6 |
| | 3 | 2%Pd/50%ZnO/$SiO_2$ | 77 | 6.6 |
| | 4 | 50%ZnO/$SiO_2$ | 170 | 3.3 |
| | 6 | 50%ZnO/$SiO_2$ | 181 | 3.7 |
| Set II | 7 | 40%Co/SBA-15 | 747 | 3.5 |

## 4.2. Reactivity Test Results

Results of ethanol steam reforming tests both in the absence and presence of oxygen or air over all catalysts except sample 5 are given below.

### 4.2.1. Ethanol Steam Reforming

Steam reforming tests were carried out over Set I catalysts. Table 8 summarizes flow rates and compositions of both liquid and gaseous mixtures sent to the system. This way, for all experiments space velocities were kept around 54000 $cm^3$/h-g catalyst using 0.1 g of catalyst (corresponding to 81000 $h^{-1}$, or space

time of 0.07 g catalyst.s/$cm^3$, 0.045 s) which is well above the values used in literature as indicated in Chapter 2.

As will be presented soon the results showed that promoted and non-promoted $ZnO/SiO_2$ catalysts used act as ethanol dehydrogenation catalysts over the temperature range of 300-500°C. Although traces of ethylene (also at 450°C), methane and carbon dioxide were observed at the reaction temperature of 500°C, each of them accounted for less than 1% of the total products including

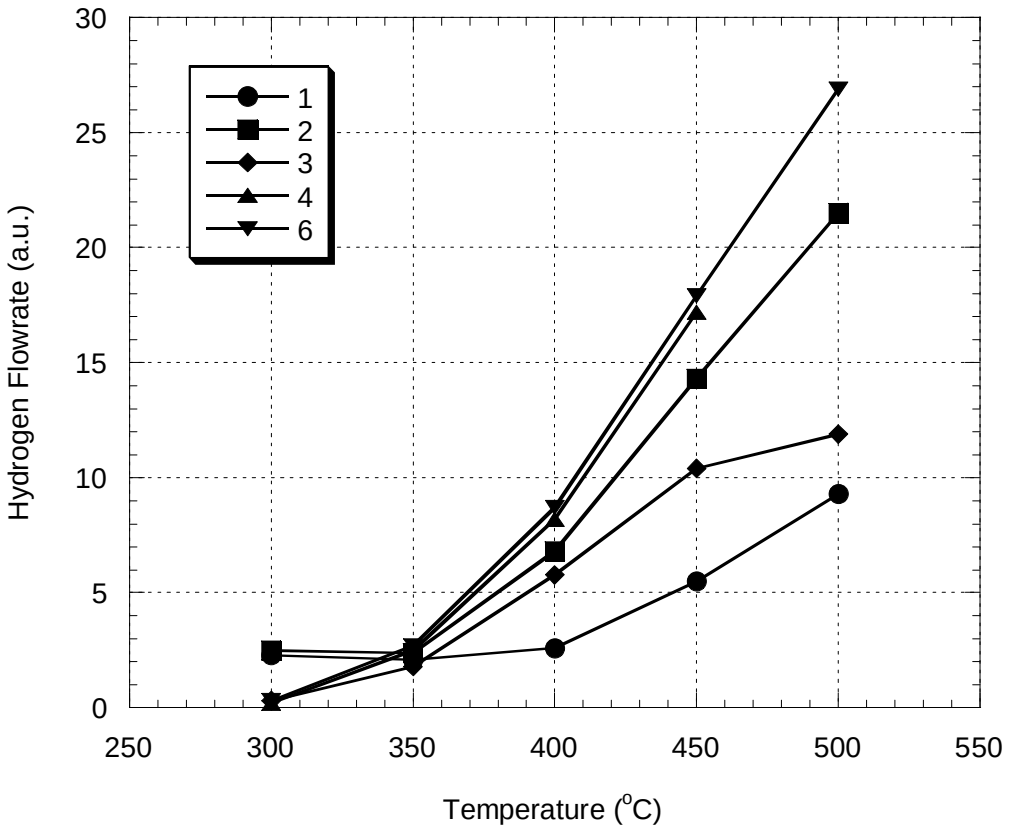


***Figure 9.*** *Effect of temperature and catalyst on hydrogen flow rate (Calculated parameters: EtOH:$H_2O$=1:3, GHSV~54000 $cm^3$/h-g catalyst, flow rate~86 $cm^3$/min. Measured parameters: Mass of catalyst=0.1 g.)*[6]

[6] Calculated parameters include gas phase parameters obtained from ideal gas law.

unconverted reactants obtained at the exit of the reactor. On the other hand, no carbon monoxide was produced. From fuel cell application's point of view, carbon monoxide-free hydrogen is something desired, yet acetaldehyde has also poisoning effect on electrodes of fuel cells as carbon monoxide do.

Figures 9 and 10 present the results obtained as hydrogen and acetaldehyde flow rates, respectively, given in arbitrary units.

As only acetaldehyde and hydrogen were produced over Set I catalysts, Figures 9 and 10 can also be regarded as selectivity plots towards hydrogen and

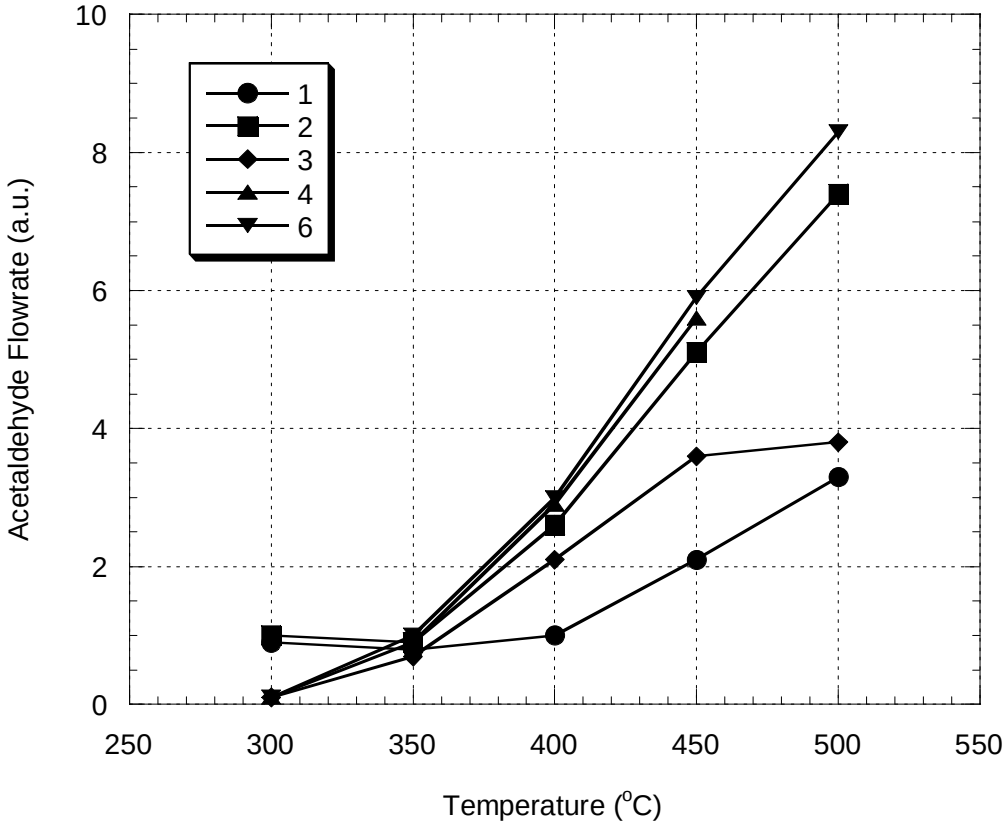


***Figure 10.*** *Effect of temperature and catalyst on acetaldehyde flow rate (Calculated parameters: EtOH:$H_2O$=1:3, GHSV~54000 $cm^3$/h-g catalyst, flow rate~90 $cm^3$/min. Measured parameters: Mass of catalyst=0.1 g.)*

acetaldehyde, respectively, and even as ethanol conversion plots, each of which having appropriate units of scale. Although not explicitly calculated and plotted, hydrogen selectivity can be defined as the ratio of the produced moles of hydrogen to the moles of hydrogen equivalent to the consumed moles of ethanol.

As seen in Figure 9, below 350°C copper-promoted catalysts (1 and 2) showed better selectivity to hydrogen. At 400°C and above this temperature, on the other hand, non-promoted catalysts appear to be superior to other catalysts in ethanol dehydrogenation. In this temperature range, 4%Cu-promoted catalyst (2) showed better results compared to Pd-promoted catalyst (3). 6%Cu-promoted catalyst (1), however, came into view with the poorest performance.

Trends in acetaldehyde flow rate, as seen in Figure 10, are very similar to those observed for hydrogen in Figure 9. This was in fact an expected result as nothing other than ethanol dehydrogenation is taking place over the catalysts: Multiplication of each and every point having arbitrary unit in Figure 10 by an average factor of 2.8 gives the data of Figure 9. This calculation also shows the consistency of the analyses carried out by GC since both hydrogen and acetaldehyde flow rates should be equal as they were produced equimolar by the only reaction, ethanol dehydrogenation.

$ZnO/SiO_2$ mixed oxide shows both acidic (Lewis acid) and basic properties [41]. Ethanol dehydrogenation occurs over basic sites of the catalyst which are capable of dissociating H-H and C-H bonds of ethanol [24,39,42]. Ethanol dehydration to ethylene, on the other hand, takes place over acidic sites [11,28,32,33,39,42]. As none of the catalysts has produced some remarkable amount of ethylene, it can be said that all Set I catalysts act as bases under reaction conditions. However, basicity of the catalysts decreases upon metal promotion.

Cu catalysts, especially Cu/ZnO, are known as active catalysts for acetaldehyde hydrogenation [12,13,16]. It has also been shown that over metallic copper, and

alumina-, silica- and zinc oxide-supported copper catalysts acetaldehyde and hydrogen can be produced with almost 100% ethanol conversion [24,25,27,28,38]. On the other hand, it has also been demonstrated that over some Pd catalysts again acetaldehyde and hydrogen were obtained as the only products [29]. Pd-Zn alloys formed during the preparation of Pd/ZnO catalysts help them exhibit similar catalytic activities with copper catalysts [37]. Acetaldehyde was also produced over Pd-Zn alloys of Pd/ZnO catalysts [38].

As such studies are available in literature it was no surprise to obtain such a product distribution over Set I catalysts. Yet, it is interesting to get poorer results with metal promoted ones. From above discussion, it can be deduced that dehydrogenation of ethanol took place over Pd/Zn alloys in sample 3. And, poor activities compared to non-promoted catalysts can be attributed to the presence of zinc silicates and metal zincates (like Pd/Zn) in pores, closed at the ends, which are, therefore, not accessible to reacting molecules. This may also explain the reason in the decrease of basic strength with metal addition.

GasChrom MP-1 used to separate analytes has low affinity to water. For this, only low levels of water in organic solvents or organics in water can be analyzed by GasChrom MP-1 [43]. The latter one applies here, and due to huge fluctuations in the areas of water peaks results of water analyses were not taken into account. As only ethanol dehydrogenation is occurring in the reactor, what comes in as water should leave without being consumed. On the other hand, ethanol and water are sent in a 1:3 mole ratio as liquid to the system. Analyses of the gaseous phase obtained at “no reaction” temperature of 200°C for all catalysts showed that this ratio was in fact smaller. This can be attributed to the erroneous water peaks and it can be assumed that the mole ratio in the liquid phase was retained also in the gaseous phase.

No reproducibility experiments were carried out with fresh catalysts. However, used samples 1 and 6 were tested once again in the setup. Again only

acetaldehyde and hydrogen constituted the product distribution. As seen in Figures 11 and 12 there observed deactivation in both catalysts.

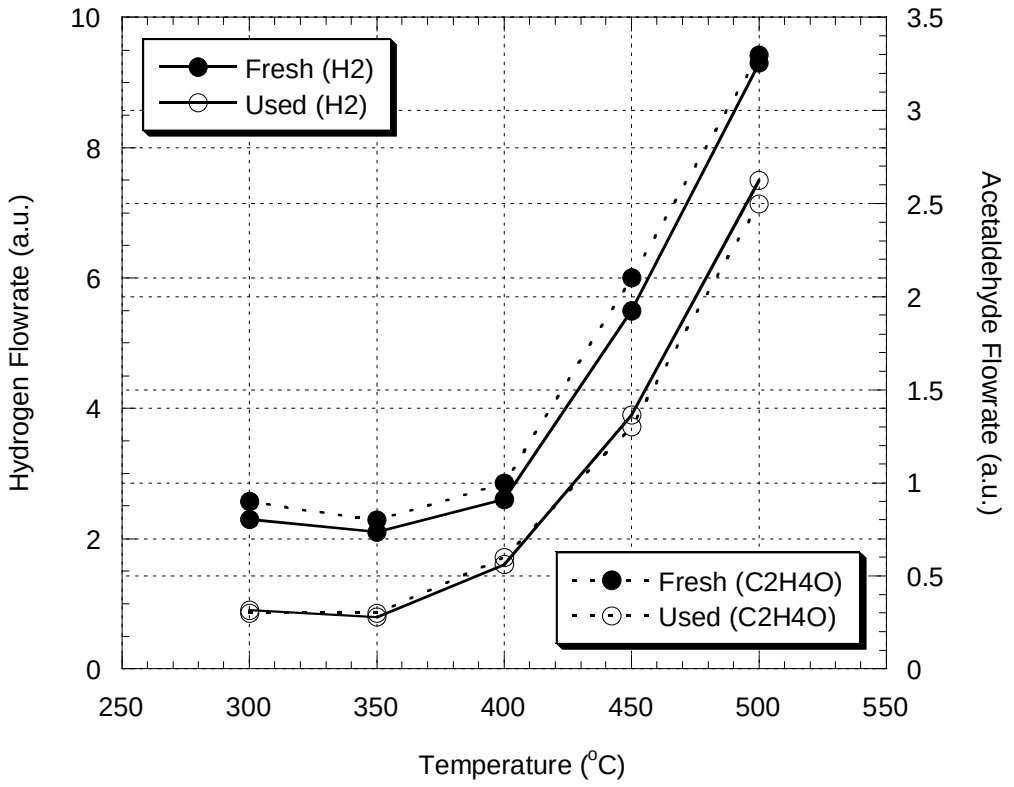


***Figure 11.*** *Deactivation in sample 1 (EtOH:$H_2O$=1:3, GHSV~54000 $cm^3$/h-g catalyst, flow rate~90 $cm^3$/min. Mass of catalyst=0.1 g.)*

Figures 9-12 were drawn without using any calibration data. They were simply plotted considering hydrogen and acetaldehyde peak areas obtained in the analyses of the gas syringe samples, and processing those data with the argon areas to take the effect of the change in the flow rate, as reaction temperature increases, into account. This way, separate scales of arbitrary units were obtained for each species. When the data were to be further processed with the

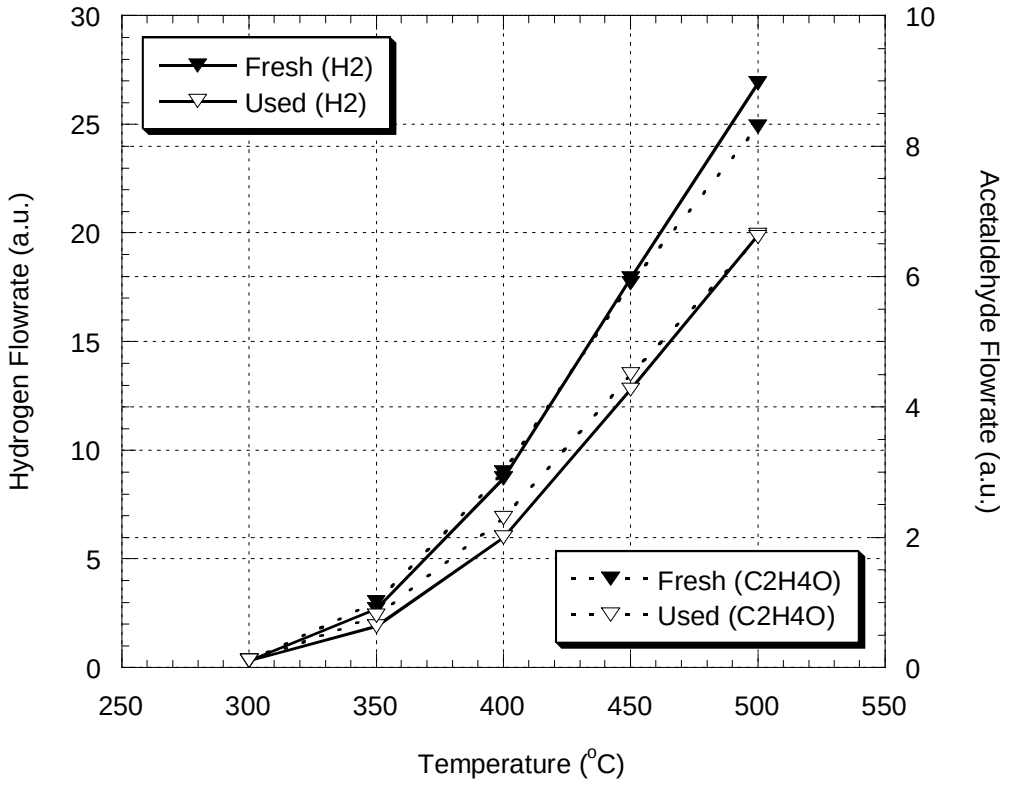


***Figure 12.*** *Deactivation in sample 6 (EtOH:$H_2O$=1:3, GHSV~54000 $cm^3$/h-g catalyst, flow rate~90 $cm^3$/min. Mass of catalyst=0.1 g.)*

calibration data, however, somewhat mistaken results would arise. Calibrations of gases, $H_2$, $CH_4$, $CO_2$ and $C_2H_4$ were done using *another* setup by gas syringes, and of $C_2H_4O$, $C_2H_6O$ and $H_2O$, by liquid syringes of *micro*liters. It is, therefore, very probable to arrive in incorrect figures after calculations using all calibration data together. Nevertheless, hydrogen flow rates of Figure 9 were re-plotted also using such calibration data as seen in Figure 13. Figure 13 is different from Figure 9. This shows that calibration appears as one of the major contributors, if there is any other, to the erroneous results. That is why, no completely-processed counterparts of Figures 9-12 will be given here.

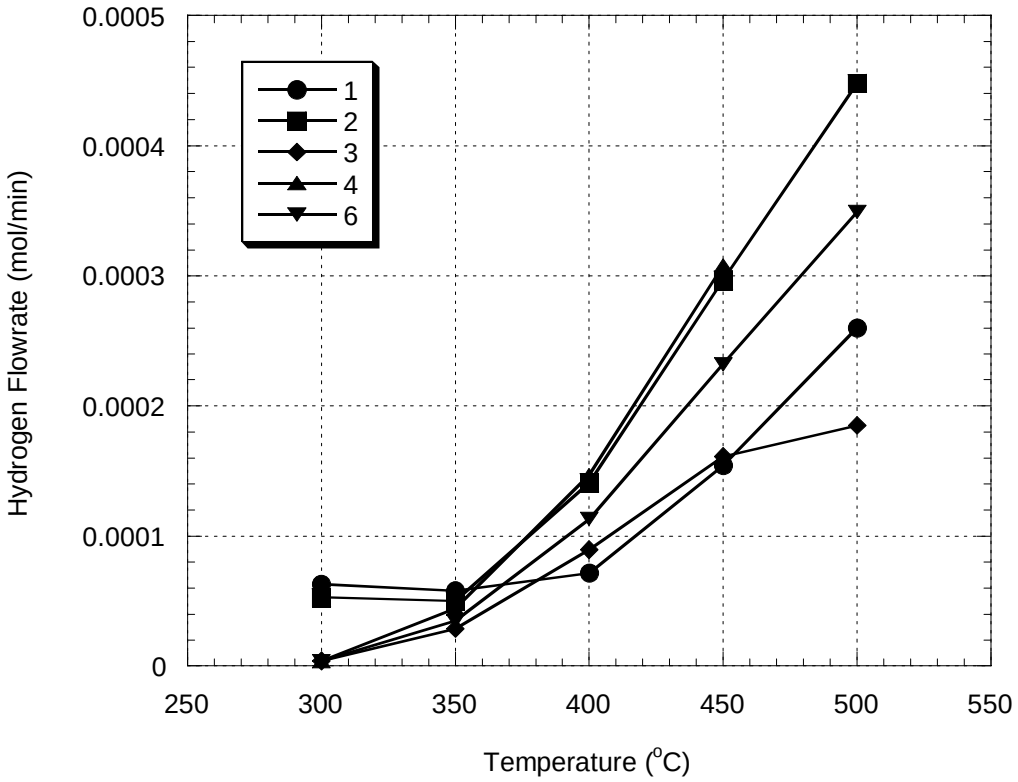


***Figure 13.*** *Effect of calibration data on hydrogen flow rate data*

All calibrations were carried out again and again with each experiment as also indicated in the sample experiment schedule available in Appendix F. Yet, all these data can be collected and evaluated by means of some statistical tools, and an *averaged* calibration data for each species can be obtained. These data relate peak area of one component directly to its flow rate (mol/min) at the reactor exit. Further information on this calculation is given in Appendix E. Figure 9 was drawn once again after manipulated with this averaged calibration data as seen in Figure 14.

Figure 14 is much similar to Figure 9 except with the plot of sample 6. So, averaged calibration data can be used for the complete evaluation of the flow data.

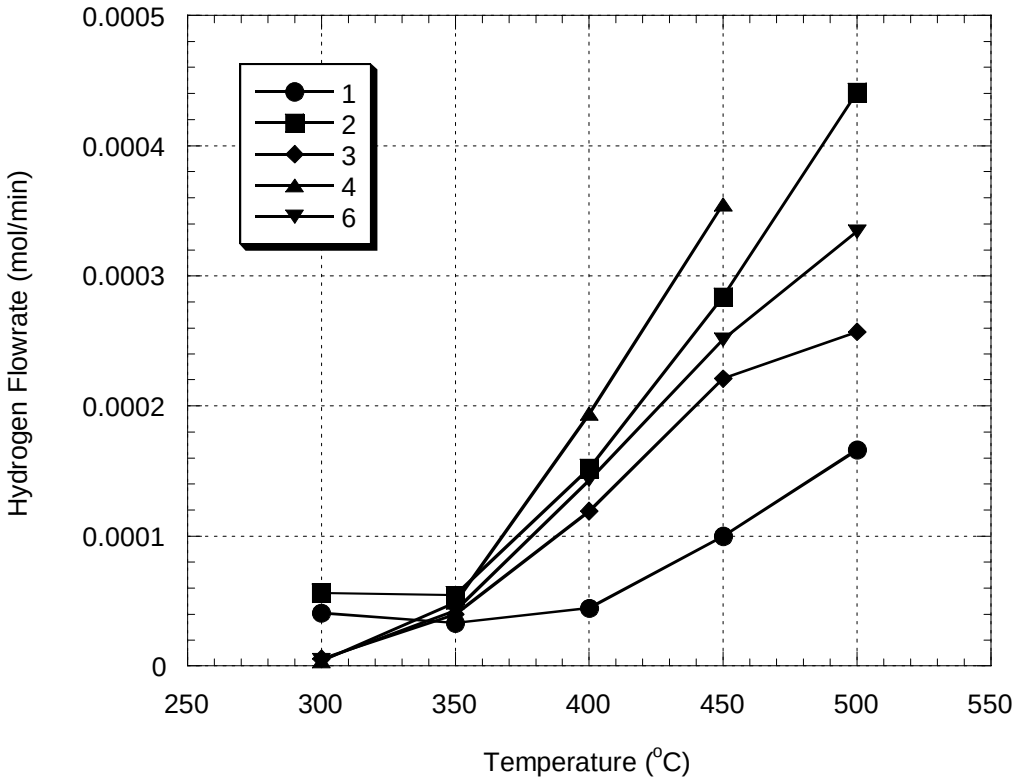


***Figure 14.*** *Hydrogen flow rates re-plotted using averaged calibration data*

Figure 15 shows the results of the time-on-stream test carried out for sample 1 at 500°C for about 48 hours, which were evaluated by averaged calibration data. As seen in Figure 15 there is a continuous decrease in ethanol flow rate. While this experiment was running it was also observed that the decrease in the ethanol-water level in the cooler of the feeding unit (Figure 6) was decreasing by time. These two observations indicate that the peristaltic pump cannot pump the same amount of liquid as time passes which is most probably due to continuous treading of the rollers on the capillary tubing. Yet, as also seen in Figure 15, this does not have much significant effect on the flow rates of hydrogen, acetaldehyde, methane and ethylene as long as there still exist some ethanol in the reacting stream. Several studies in the literature [31-33] have reported a decrease in ethanol conversion which did not affect the selectivities of

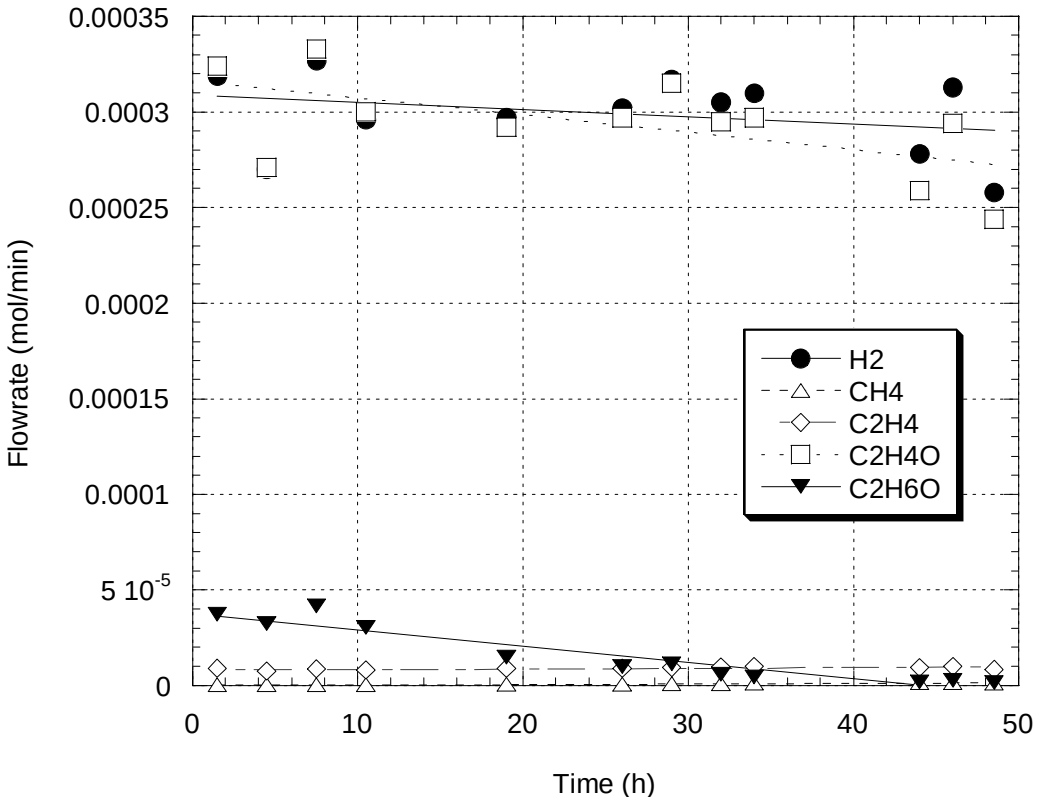


***Figure 15.*** *Time-on-stream test of sample 1 at 500℃ (Lines shown are linear curve fits.)*

the products during time-on-stream tests of different catalysts. The situation here is not fully same with what has been described in those studies. Firstly, a decrease in ethanol conversion means an increase in its exit flow rate, and here, it is just the opposite. Secondly, unaffected selectivities do not always mean that the total flow rate of the products keeps constant. Decrease in the flow rates of the reactants decreases productivity, but at the same time, this also decreases the space velocity which promotes productivity. Therefore, unaffected flow rates or selectivities of hydrogen, acetaldehyde, and other minor products in the time-on-stream test can be attributed to this cancellation effect. On the other hand, almost constant flow rates of Figure 15 indicate that, contrary to what has been discussed on Figures 11 and 12, there is no catalyst deactivation on-stream.

Assuming similar behavior in the pumping of the liquid feed to the system in every experiment, the data of the previous experiments are still comparable. This can be seen in the hydrogen and acetaldehyde flow rates obtained by samples 4 and 6, which are almost equal at each temperature, as seen in Figures 9 and 10, respectively. This was an expected result as the compositions of those catalysts do not differ from each other. Decrease in the ethanol-water amount fed to the system, however, indicates a decrease in the space velocities as mentioned above. So, calculated space velocities were not, or at least, might not be what were obtained at the end of the experiments. It is expected to gain a higher selectivity towards hydrogen under lower space velocities; therefore, flow rates of the products at higher temperatures shown in the previous figure may appear to be higher than what should be under *calculated* space velocities[7].

Due to the discussion above no explicit ethanol conversion plots and no explicit hydrogen selectivity plots were given here, as Figures 9 and 10 already give an insight to them.

Elemental carbon balance was also carried out for all experiments done using both same-day calibration data and averaged calibration data. Carbon in the carbon-containing species at the reactor exit at every temperature is compared with the carbon in the ethanol exiting the reactor at 200°C, the no-reaction temperature. Percent errors in carbon balances are given in Table A.6 in Appendix D. A positive figure can be expressed as a "carbon *consumption* or accumulation," and a negative figure as a "carbon *generation*."

More positive values at higher temperatures would befit to the previous discussions as ethanol pumping rate is known to decrease with time (or, here, temperature) and as a possible coking action would result in a carbon accumulation. However, Table A.6 presents a set of data which is just the opposite. One reason of this can be a possible distillation effect in the bulb of the

[7] All steam reforming tests were done by increasing the reactor temperature after completing analyses in one temperature.

feeding unit which causes more water to go into reactor at the beginning of the experiments. Yet, this was proved to be irrelevant by the ethanol decrease of Figure 15[8]. As it was also observed almost equal hydrogen and acetaldehyde flow rates in the time-on-stream test, the only reason left can then be the incorrect calibrations of ethanol, which is one of the two major carbon-containing species other than acetaldehyde, done by using liquid syringes of microliters.

### 4.2.2. Autothermal Reforming

Autothermal reforming experiments were done with samples 2 and 3 of Set I, and with the Set II catalyst, sample 7. Again, flow rates and compositions of both liquid and gaseous phases of the reacting medium are given in Table 8. Again, 0.1 g catalysts were used in the experiments. Calculated space velocities for Set I catalyst tests remained the same as given in §4.2.1. For sample 7, however, two different tests were performed, one with high space velocity, and one with low space velocity. For the former test, space velocity was kept almost same with all previous experiments, 52000 $cm^3$/h-g catalyst which corresponds, however, to 20000 $h^{-1}$ due to high packing volume[9]. Low space velocity, on the other hand, equals to 31000 $cm^3$/h-g catalyst (12000 $h^{-1}$)[10]. These are all calculated values, and as shown in the previous section, they do not remain same throughout the whole experiment and, unfortunately, decrease.

Results showed that presence of oxygen in the reacting stream changed the product distribution a little bit by adding three more products. Analyses of the condensates collected in the condenser for disposal purposes showed that two of those species are in liquid phase under room temperature. Unfortunately, those species could not be identified. On the other hand, traces of species like diethyl

[8] So, the assumption of same gaseous composition with that in liquid is still valid.
[9] Corresponding to space time of 0.07 g catalyst.s/$cm^3$ or 0.18 s.
[10] Corresponding to space time of 0.12 g catalyst.s/$cm^3$ or 0.3 s.

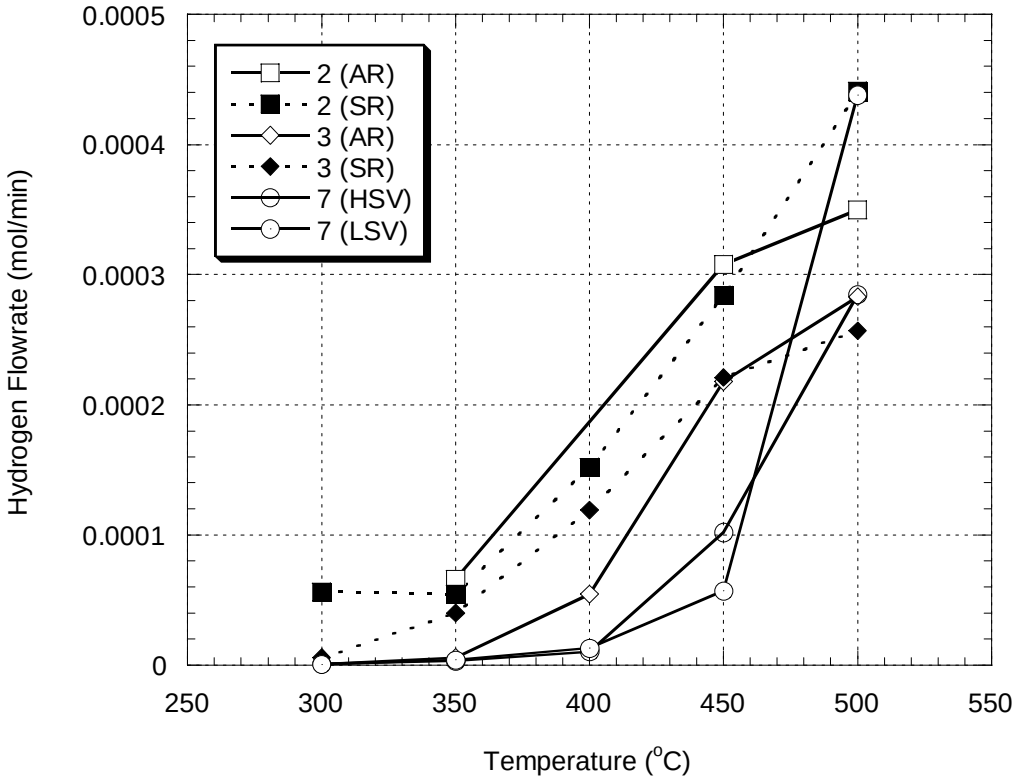


***Figure 16.*** *Effect of temperature and catalyst on hydrogen flow rate (AR: Autothermal Reforming. SR: Steam Reforming. HSV: AR with high space velocity. LSV: AR with low space velocity. Calculated parameters: EtOH:$H_2O$=1:3; GHSV~54000 $cm^3$/h-g catalyst (SR, AR, HSV) ~31000 $cm^3$/h-g catalyst (LSV); flow rate~90 $cm^3$/min (SR) ~86 $cm^{3/}$min (AR, HSV) ~51 $cm^3$/min (LSV). Measured parameters: Mass of catalyst=0.1 g.)*

ether, ethyl acetate, ethane, acetic acid, acetone or formaldehyde reported in the literature were not observed.

As there were some major unidentified peaks in the analyses, it would be appropriate to present the results of the experiments in a fashion done in the previous section. Figures 16 to 20 illustrate the exit flow rates of hydrogen, acetaldehyde, methane, carbon dioxide and ethylene, respectively, obtained over

each catalyst[11]. Those of steam reforming tests done over samples 2 and 3 were also included in the figures for comparison purposes. It is worth noting that all data were evaluated using averaged calibration data of the previous section as argon could not be used for total flow rate determinations as mentioned in §3.3. Yet, analyses of oxygen could not be done properly either as the thermal conductivity of the reference gas, nitrogen, is near to that of oxygen.

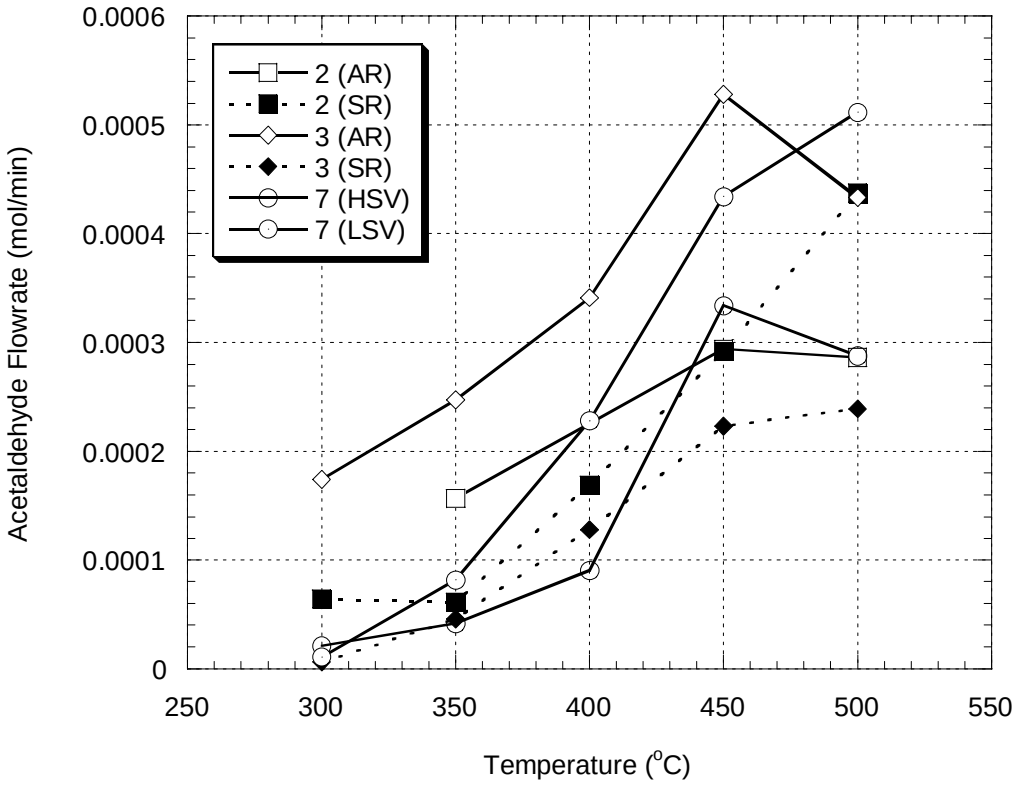


***Figure 17.*** *Effect of temperature and catalyst on acetaldehyde flow rate*[11]

It is interesting that no carbon monoxide was produced in the experiments. Although none of the catalysts show a specific trend as seen in the figures, it is

[11] Experimental conditions and explanations to abbreviations used are given in Figure 24.

also strange enough to observe higher acetaldehyde flow rates compared to hydrogen. Acetaldehyde flow rates would be expected to be lower since acetaldehyde usually acts as an intermediate in the production of hydrogen. This is most probably a consequence of evaluation of raw data with the averaged calibration data as it is very unlikely for hydrogen to take place in the formation of larger molecules, maybe one or more of those unidentified species. As no carbon monoxide was also produced effect of water-gas shift reaction is eliminated. Therefore, it is reasonable to compare the catalysts on the basis of each species produced as done in Figures 16-20.

As seen in Figure 16, steam reforming over samples 2 and 3 still gives higher hydrogen productivity except for authermal reforming of sample 2 which seems to be better. Both high space velocity and low space velocity experiments of

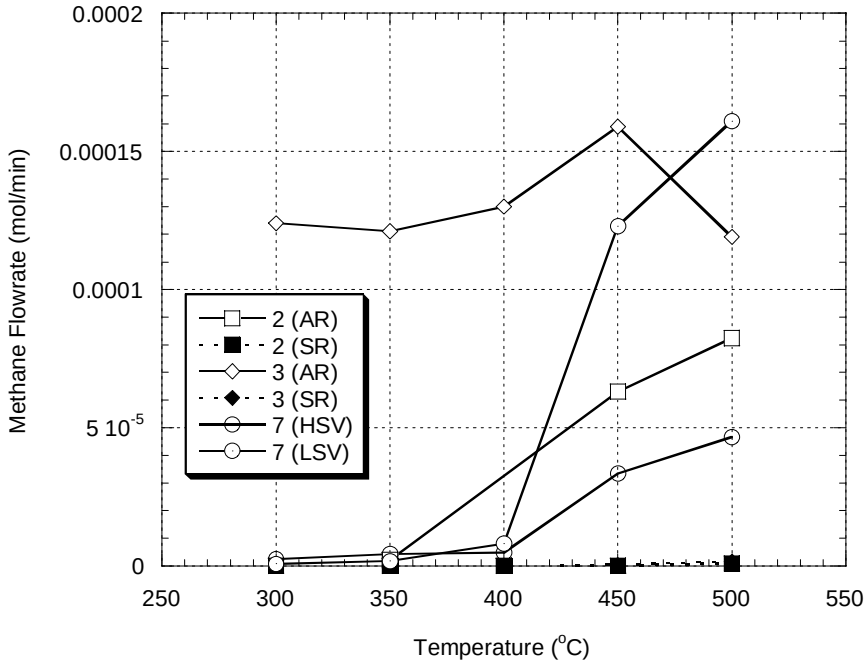


***Figure 18.*** *Effect of temperature and catalyst on methane flow rate*[11]

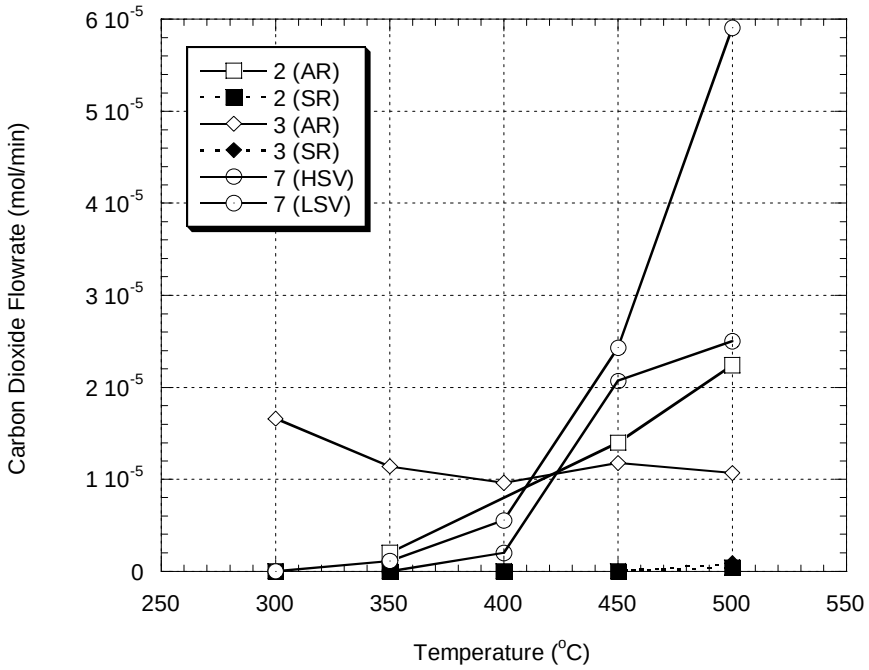


***Figure 19.*** *Effect of temperature and catalyst on carbon dioxide flow rate*[11]

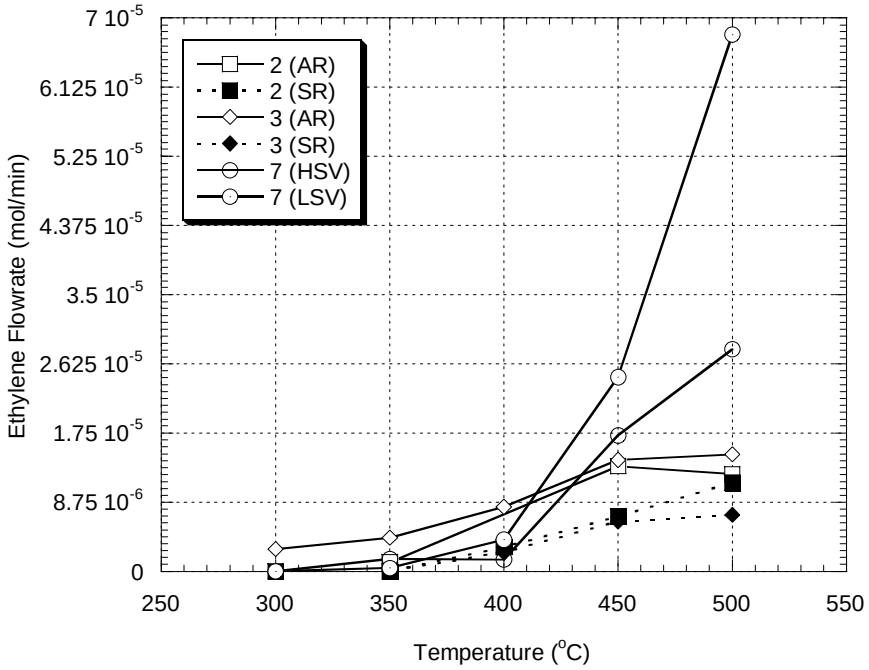


***Figure 20.*** *Effect of temperature and catalyst on ethylene flow rate*[11]

cobalt catalyst, however, showed the poorest selectivity towards hydrogen. Yet, higher hydrogen flow rates were obtained when running with low space velocity.

On the other hand, formation of ethylene, methane and carbon dioxide increased with the presence of oxygen. Cobalt catalyst showed higher productivity towards ethylene and carbon dioxide. Moreover, by decreasing the space velocity higher flow rates for all products were obtained over the cobalt catalyst. Here, it is worth noting that experiment for low space velocity cobalt testing was started at 500°C and ended up at 200°C.

# CHAPTER 5

# SUMMARY AND CONCLUSIONS

Decrease in the fossil fuel reserves on which more than 85% of world's energy depends on today, and new regulations brought on emission control have led the way to studies on alternative fuels. Hydrogen production through ethanol steam reforming is one such new research area.

ZnO catalysts are known as methanol synthesizing catalysts from syngas, hydrogen and carbon monoxide. From the principle of microkinetic reversibility, catalysts promote also backward reaction as they promote forward reaction. Starting from this point, it may be possible to produce hydrogen with high selectivities from methanol and even ethanol over ZnO catalysts.

Ethanol is a renewable feedstock. According to studies available in the literature when ethanol is reformed with steam over suitable catalyst, hydrogen can be produced with carbon dioxide; however, no additional carbon dioxide is emitted to the atmosphere, and instead, carbon in ethanol is only recycled in nature to be used again in photosynthesis.

In the first part of this study, ethanol steam reforming reaction was tested over sol-gel-prepared non-promoted, and Pd- or Cu-promoted zinc oxide catalysts supported on silica in a developed experimental setup. Analyses showed similar results with those in the literature. These catalysts acted as ethanol dehydrogenation catalysts in the temperature range of 300-500°C and under other experimental conditions. Hydrogen selectivity was higher over non-promoted catalysts at high temperatures and over Cu-promoted ones at low temperatures. Pd and Cu promotion would be expected to bring superiority to

ZnO catalysts; however, it didn't come out to be so. The reason of this can be attributed to the presence of possible zinc silicates and metal zincates enclosed in closed pores which are not reachable to adsorbed gas molecules. These closed pores can also be the reason in the decrease in BET surface area and basic strength with metal addition to the catalyst.

Deactivation due to air contact was observed when used catalysts were tested once again later in the setup. On the other hand, there was no deactivation on-stream.

It was further detected that selectivities were not affected much by the decrease in ethanol and water amount in the reacting medium as long as there exist some.

In the second part of the study, steam reforming experiments were carried out this time with the presence of oxygen or air over those promoted zinc oxide catalysts and over SBA-15-supported cobalt catalyst. These autothermal reforming tests showed similar hydrogen selectivities over promoted zinc oxide catalysts when compared with their steam reforming results. On the other hand, hydrogen selectivities were lower over the cobalt catalyst. Formation of side products like methane, carbon dioxide, ethylene, and three more species which could not be identified increased in autothermal reforming experiments.

Formation of carbon monoxide was not seen in any of the experiments.

# CHAPTER 6

# RECOMMENDATIONS

As mentioned previously, setting up a proper feeding unit and trying to establish a working experimental system took about three fourth of the time spent on this study as dealing with three-phase systems is not an easy task. Still, results of the experiments revealed the problems existing with the feeding unit due to changing pumping rate of the peristaltic pump. A syringe pump could have been used instead of a peristaltic pump in the setup to obtain a steady feeding.

On the other hand, carrying the analytes to GC in a gas syringe was not an easy task either. First of all, before taking samples from sampling vessel into the syringe, syringe was heated by a heating gun not to let any condensation to happen within the syringe. This was something reducing the lifespan of the syringe as heating may harm the Teflon structures. So, one should be as quick as possible not to lose time while taking the sample and injecting it to GC. Secondly, the injection port of the GC was equipped with a septum as the sampling vessel, and septum particles were, most of the time, blocking the needles of the syringes. Trying to take those particles out of the needle was something annoying and time consuming as it was causing termination of the experiment to delay. For this, analytes should have been sent to GC on-line instead of by using syringes. However, this time the line from the reactor to the injection port of the GC would need to be surrounded by a longer heating tape or by extra heating tapes which was not possible due to unavailability.

A longer column had to be used, and low flow rates along with a temperature ramp had to be applied in GC in order to separate species like hydrogen, carbon monoxide, methane and carbon dioxide which come out of the column rather

quickly while trying to decrease the retention time of the final component, ethanol, as much as possible. As a result of this, one analysis lasted for about 1 hour. For this, analysis time was the major reason in having *long* experiments usually lasting for more than one day. Incorrect injections due to condensation in the syringe or plugged syringe needle also caused additional delays.

On the other hand, the most unpleasant situations occurred when the electricity was cut. Many analyses and experiments were terminated as a result of electricity cuts. For this, laboratories should be equipped with generators as sudden voltage changes not only terminate the experiments but also give harm to expensive equipments like GCs.

Analyses of autothermal reforming experiments could not be carried out completely as argon used as the total flow determinant could not be separated from oxygen in the column. Sending helium instead of argon would not solve the problem either as this time helium, hydrogen and carbon monoxide would not be separated. Changing the reference gas of the GC to helium and using nitrogen in the setup both as the carrier gas and the internal standard would not be effective also since hydrogen would not be analyzed properly due to very near thermal conductivities with the reference gas, helium. The only solution could be a concurrent analysis in another GC.

Finally, a more practical method needed to be used for calibration as the major contributor to erroneous results was shown to be the calibration data. For instance, a volumetric calibration of feed and products could have been carried out in which volumetric decrease in the ethanol-water solution of the cooler with time could have been recorded, and several sets at the “no-reaction” temperature could have been carried out. This way, ethanol could have been more accurately calibrated.

# REFERENCES


1. Energy Information Administration (EIA), *International Energy Annual 2001*, Washington, D.C. (2003)

2. Energy Information Administration (EIA), *System for the Analysis of Global Energy Markets* (2004)

3. Campbell, C.J. and Laherrere, J.H., "The End of Cheap Oil," *Scientific American*, 78 (March 1998)

4. Aupretre, F., Descorme, C., Duprez, D., *Catalysis Communications*, **3**, 263 (2002)

5. The Cooperative Research Centre for Greenhouse Accounting, "About Greenhouse," *http://www.greenhouse.crc.org.au/crc/ecarbon/history.htm* (Last accessed: June 2005)

6. Austin, G.T., *Shreve's Chemical Process Industries*, 5th Ed., Ch. 7, 101, McGraw-Hill (1984)

7. Deluga, G.A., Salge, J.R., Schmidt, L.D., Verykios, X.E., *Science*, **303**, 993 (2004)

8. *Bioethanol – the Climate-Cool Fuel: Biofuels for the Global Environmental Fact Sheet*, National Renewable Energy Laboratory, Golden, CO, US (1997)

9. Trimm, D.L. and Önsan, Z.I., *Catalysis Reviews*, **43**, 1&2, 31 (2001)

10. *The Clean Cities Alternative Fuel Price Report*, U.S. Department of Energy (November 26, 2004)

11. Claus, P., Lucas, M., Lücke, B., *Applied Catalysis A: General*, **79**, 1 (1991)

12. Nunan, J.G., Bogdan, C.E., Klier, K., Smith, K.J., Young, C.W., Herman, R.G., *Journal of Catalysis*, **113**, 410 (1988)

13. Nunan, J.G., Herman, R.G., Klier, K., *Journal of Catalysis*, **116**, 222 (1989)

14. Klier, K., Beretta, A., Sun, Q., Feeley, O.C., Herman, R.G., *Catalysis Today*, **36**, 3 (1997)

15. Smith, K.J., Young, C.W., Herman, R.G., Klier, K., *Industrial & Engineering Chemistry Research*, **30**, 61 (1991)

16. Ehwald, H., Ewald, H., Gutschick, D., Hermann, M., Miessner, H., Öhlmann, G., Schierborn, E., *Applied Catalysis*, **76**, 153 (1991)

17. Garcia, E.Y. and Laborde, M.A., *International Journal of Hydrogen Energy*, **16**, 5, 307 (1991)

18. Vasudeva, K., Mitra, N., Umasankar, P., Dhingra, S.C., *International Journal of Hydrogen Energy*, **21**, 1, 13 (1996)

19. Fishtik, I., Alexander, A., Datta, R., Geana, D., *International Journal of Hydrogen Energy*, **25**, 31 (2000)

20. Ioannides, T., *Journal of Power Sources*, **92**, 17 (2001)

21. Tsiakaras, P. and Demin, A., *Journal of Power Sources*, **102**, 210 (2001)

22. Choi, Y. and Stenger, H.G., *Applied Catalysis B: Environmental*, **38**, 259 (2002)

23. Cheng, W.H., *Applied Catalysis A: General*, **130**, 13 (1995)

24. Reddy, B.M., Reddy, E.P., Manohar, B., *Journal of the Chemical Society-Chemical Communications*, 14 (1992)

25. Freni, S., Mondello, N., Cavallaro, S., Cacciola, G., Parmon, V.N., Sobyanin, V.A., *Reaction Kinetics and Catalysis Letters*, **71**, 1, 143 (2000)

26. Rostrup-Nielsen, J.R., *Catalysis, Science and Technology*, **5**, Ch. 1, Berlin (1984)

27. Mariño, F.J., Cerrella, E.G., Duhalde, S., Jobbagy, M., Laborde, M.A., *International Journal of Hydrogen Energy*, **23**, 12, 1095 (1998)

28. Mariño, F., Baronetti, G., Jobbagy, M., Laborde, M., *Applied Catalysis A: General*, **238**, 41 (2003)

29. Galvita, V.V., Semin, G.L., Belyaev, V.D., Semikolenov, V.A., Tsiakaras, P., Sobyanin, V.A., *Applied Catalysis A: General*, **220**, 123 (2001)

30. Galvita, V.V., Belyaev, V.D., Semikolenov, V.A., Tsiakaras, P., Frumin, A., Sobyanin, V.A., *Reaction Kinetics and Catalysis Letters*, **76**, 2, 343 (2002)

31. Freni, S., *Journal of Power Sources*, **94**, 14 (2001)

32. Fatsikostas, A.N., Kondarides, D.I., Verykios, X.E., *Chemical Communications*, 9, 851 (2001)

33. Liguras, D.K., Kondarides, D.I., Verykios, X.E., *Applied Catalysis B: Environmental*, **43**, 345 (2003)

34. Cavallaro, S., Chido, V., Freni, S., Mondello, N., Frusteri, F., *Applied Catalysis A: General*, **249**, 119 (2003)

35. Llorca, J., Homs, N., Sales, J., Ramirez de la Piscina, P., *Journal of Catalysis*, **209**, 306 (2002)

36. Cavallaro, S. and Freni, S., *International Journal of Hydrogen Energy*, **21**, 6, 465 (1996)

37. Takezawa, N. and Iwasa, N., *Catalysis Today*, **36**, 45 (1997)

38. Iwasa, N., Yamamoto, O., Tamura, R., Nishikubo, M., Takezawa, N., *Catalysis Letters*, **62**, 179 (1999)

39. Llorca, J., Ramirez de la Piscina, P., Sales, J., Homs, N., *Chemical Communications*, 7, 641 (2001)

40. Cannas, C., Mainas, M., Musinu, A., Piccaluga, G., *Composites Science and Technology*, **63**, 8, 1187 (2003)

41. Tanabe, K., Misono, M., Ono, Y., Hattori, H., *Studies in Surface Science and Catalysis*, **51**, 27 (1989)

42. Tanabe, K., Misono, M., Ono, Y., Hattori, H., *Studies in Surface Science and Catalysis*, **51**, 215 (1989)

43. *Chromatography Catalog 450*, 173, Alltech (1999)

44. Sandler, S.I., *Chemical and Engineering Thermodynamics*, 3rd Ed., 744, Wiley (1999)

45. Larminie, J. and Dicks, A., *Fuel Cell Systems Explained*, Ch. 3, 37, Wiley (2000)

46. Peters, M.S. and Timmerhaus, K.D., *Plant Design and Economics for Chemical Engineers*, 4th Ed., 800, McGraw-Hill (1991)

47. Brinker, C.J., Keefer, K.D., Schaefer, D.W., Assink, R.A., Kay, B.D., Ashley, C.S., *Journal of Non-Crystalline Solids*, **63**, 45 (1984)

# APPENDIX A

# ECONOMIC ANALYSIS

*Theory*

An economic analysis was carried out for a system consisting of an ethanol steam reformer and a proton exchange membrane fuel cell (PEMFC).

Figure A.1 shows a schematic representation of a PEMFC. Hydrogen from the reformer is fed to the anode of the fuel cell, and pure oxygen or air is fed to the cathode. An electron flow takes place in the external circuit as a consequence of the anodic and cathodic reactions, which is nothing but electricity.

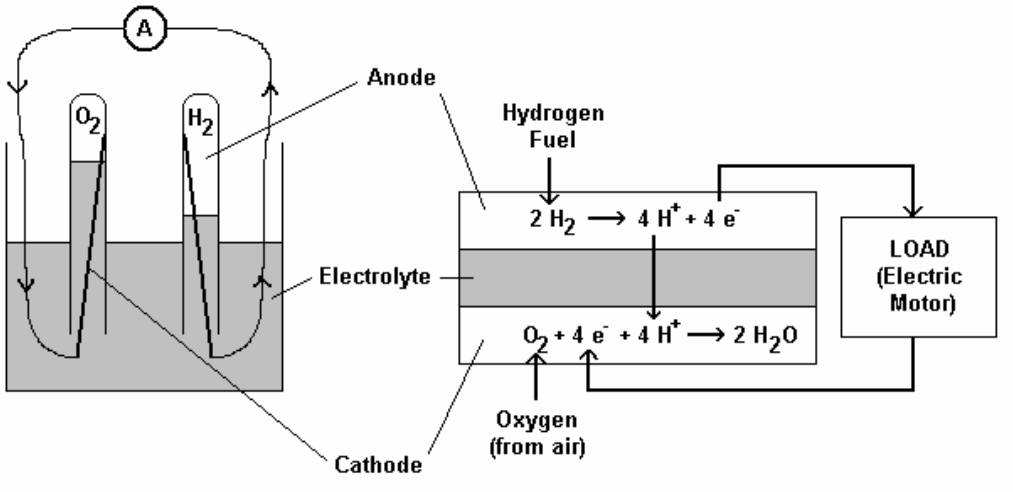


***Figure A.1.*** *Proton exchange membrane fuel cell (PEMFC)*

Studies available in the literature have shown that it is possible to obtain almost complete conversions in ethanol steam reforming with very high hydrogen selectivities at elevated temperatures. Therefore, at the very beginning of the analysis it was assumed that complete reaction to carbon dioxide and hydrogen was taking place in the reformer of the system. Reactants, ethanol and water of the reformer, and air of the fuel cell, were then assumed to be fed to the system at room temperature. Operating temperature of PEMFC was further assumed to be 75°C which is a typical value. Temperature of the effluent from the reformer leaving at a high reforming temperature should then be lowered to 75°C. Therefore, it is reasonable to assume for the steam reforming as taking place at 75°C since heat necessary to increase the temperature of ethanol and water in the reformer high above 75°C would well be gained back while lowering the temperature of carbon dioxide and hydrogen to 75°C.

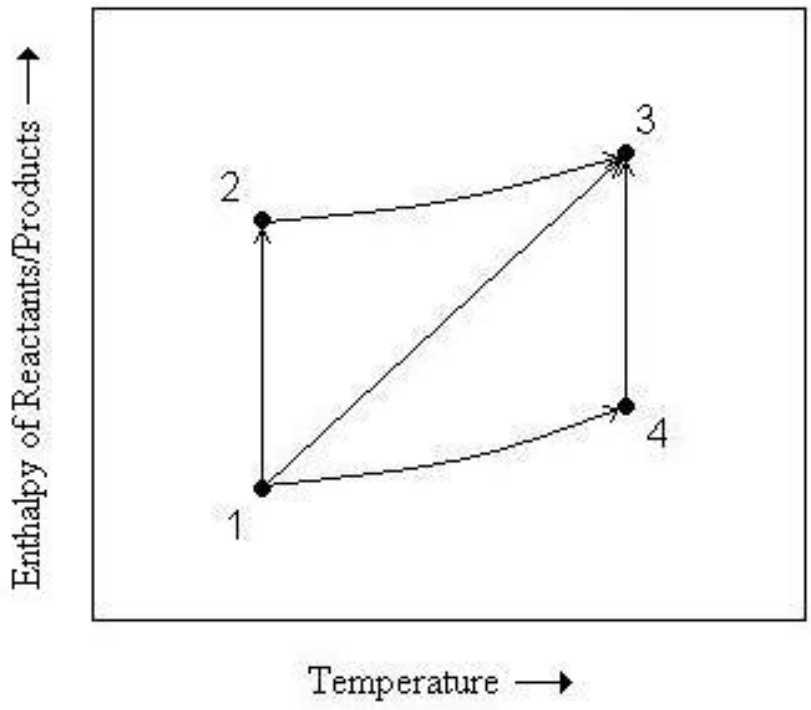


***Figure A.2.*** *Enthalpy-temperature diagram*

Figure A.2 shows a representative enthalpy-temperature diagram for reformer reactants and products. Ethanol steam reforming is an endothermic reaction; therefore, points 1 and 4 represent heats of reactants at 25°C (room temperature) and at 75°C, respectively. Similarly, points 2 and 3 represent heats of products again at 25°C and 75°C, respectively. In the reformer, ethanol and water are firstly heated to 75°C at which temperature, then, complete reaction takes place, as shown in the figure by the path from 1 to 3. Calculations can be carried out also by following the path from 1 to 4, and then, the path from 4 to 3. Therefore, in the analysis, reaction heat of ethanol steam reforming at 25°C, and sensible heats of carbon dioxide and hydrogen, and also of air, necessary to increase their temperature from 25°C to 75°C were used. Values of reaction and sensible heats are listed in Table A.1.

***Table A.1.*** *Reaction heat and sensible heats used in the analysis [44]*

| **Heat of reaction at 25°C (kJ/mol)** | $C_2H_5OH + 3H_2O \rightarrow 2CO_2 + 6H_2$ | | |
|---|---|---|---|
| | 173.5 | | |
| **Sensible heat to raise temperature from 25°C to 75°C (J/mol)** | $CO_2$ | $H_2$ | Air |
| | 1907 | 1443 | 1458 |

To relate the voltage of the fuel cell to its current density, on the other hand, the equation available in the publication by Larminie and Dicks [45], which brings together all the irreversibilities in the fuel cell like fuel crossovers, ohmic loses, etc., was adapted:

$$V = E - (i + i_n)r - A\ln\left(\frac{i + i_n}{i_0}\right) + B\ln\left(1 - \frac{i + i_n}{i_1}\right) \tag{27}$$

where, E: reversible open circuit voltage,

$i_n$: internal and fuel crossover equivalent current density,

A: slope of the Tafel line,

$i_0$: either exchange current density at the cathode if the cathodic overvoltage is much greater than the anodic, or a function of both exchange current densities,

B: constant related to mass transfer overvoltage,

$i_l$: limiting current density at the electrode which has the lowest current density,

r: area specific resistance.

Typical values for the constants of this equation were also taken from the same source as listed in Table A.2.

***Table A.2.*** *Typical constants in equation (27) for PEMFC [45]*

| Constant | Typical value for PEMFC |
|---|---|
| E (volt) | 1.2 |
| $i_n$ (mA/cm$^2$) | 2 |
| R (kΩ/cm$^2$) | $30\times10^{-6}$ |
| $i_0$ (mA/cm$^2$) | 0.067 |
| A (volt) | 0.06 |
| B (volt) | 0.05 |
| $i_l$ (mA/cm$^2$) | 900 |

Ethanol and electricity costs were taken from Peters and Timmerhaus [46]. Table A.3 lists the values of them. On the other hand, heat is always generated in

a fuel cell. In this analysis, the amount of heat which was calculated by the following equation [45] was considered as electricity and included in the analysis as a "money gained:"

$$Heating\ rate = n\,I\left(1.25 - V_c\right) \tag{28}$$

where, n: number of cells in the fuel cell,

I: current,

$V_c$: average voltage of one cell.

***Table A.3.*** *Ethanol and electricity costs [46]*

| Item | Cost |
|---|---|
| Ethanol | $2/gal |
| Electricity | $0.035-$0.13/kWh |

It was presumed that water vapor was finally produced in the fuel cell. However, nothing further about this steam was taken into consideration in the analysis. Moreover, no purchase cost or no purification cost for water fed to the reformer was taken into account.

Each calculation in the analysis was done against a current density of the fuel cell. For a specific electrode area, current, and then via equation 27, fuel cell voltage, and hence, the amount of electricity produced were calculated. Heat generated in the fuel cell was then obtained from equation 28. Altogether these figures sum up as the total money earned at the end. To calculate the operating

cost, or in other words, the total money spent, hydrogen fuel usage was calculated using the following formula:

$$Hydrogen\ usage = \frac{I}{2F} \tag{29}$$

where, I: current,

F: Faraday constant.

From this value, amounts of ethanol and air used in the system were obtained through reaction stoichiometries. Finally, ethanol cost together with sensible heat costs and reaction heat cost gave the operating cost.

Same analysis was also carried out for ethanol autothermal reforming. Again complete conversion was assumed to carbon dioxide and hydrogen. Different from steam reforming case, autothermal reforming also uses oxygen in the reformer. So, it was assumed that air was also fed to the reformer as the oxygen source. However, then, sensible heat change of nitrogen in the reformer was included in the calculations as well.

*Results*

Deluga et al. [7] made use of a perfect fuel cell assuming that hydrogen fed to the fuel cell is totally converted into steam and the exothermic heat of this process is totally converted into electricity in their economic analysis. Although there are studies reporting more than 95% ethanol conversion with very high hydrogen selectivity in a reformer as also taken to be so in the study of Deluga et al., there is no such perfect fuel cell. So, a more realistic analysis was carried out for ethanol steam reforming.

Figures A.3 and A.4 illustrate the results of the economic analysis carried out for one-hour operation of a reformer-fuel cell system equipped with a small

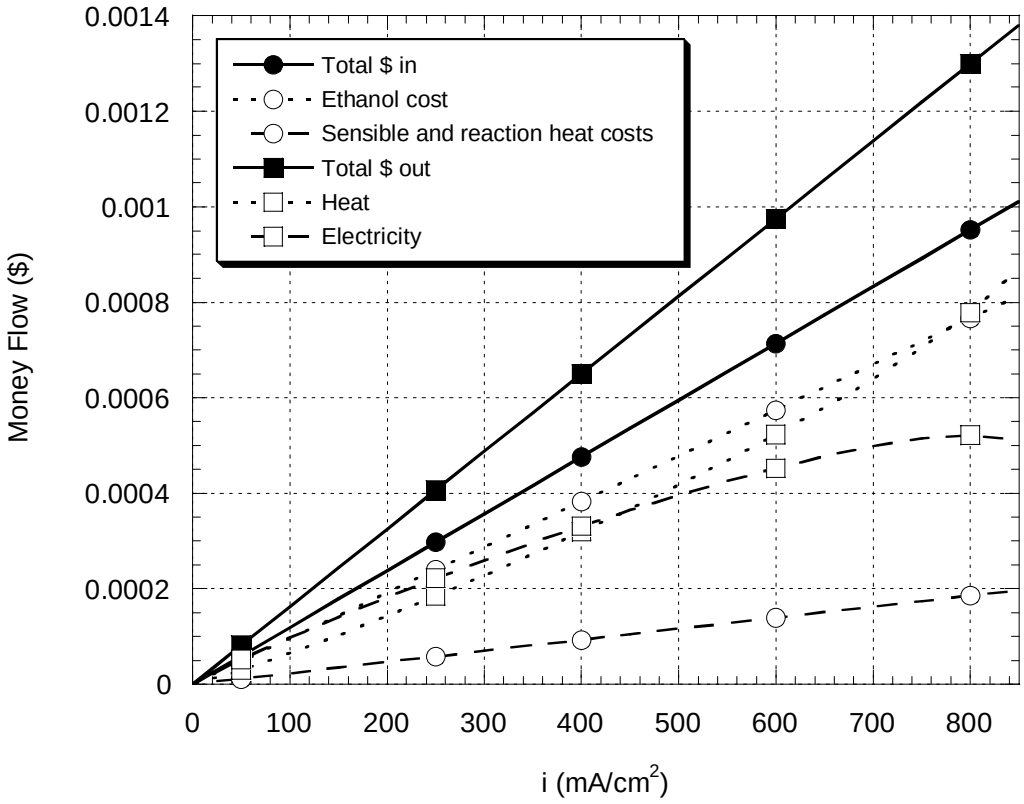


***Figure A.3.*** *Money flow scheme for a system of an ethanol steam reformer and a small PEM cell of area 10 cm$^2$ (See text for details.)*

electrode having 10 cm$^2$ area. "Total $ in" stands for the money spent to operate the system. It is, in other words, the operating cost which includes the ethanol cost along with the sensible and reaction heat costs. Similarly, "Total $ out" is used for the amount of money earned at the end out of this system. This value comprises the heat generated in the fuel cell which is included as electricity, and the electricity produce by the fuel cell. Cost of electricity was taken to be $0.13/kWh.

As seen in the figures ethanol cost makes up most of the operating cost of the system which is due to the amount of energy used to remove all water content in

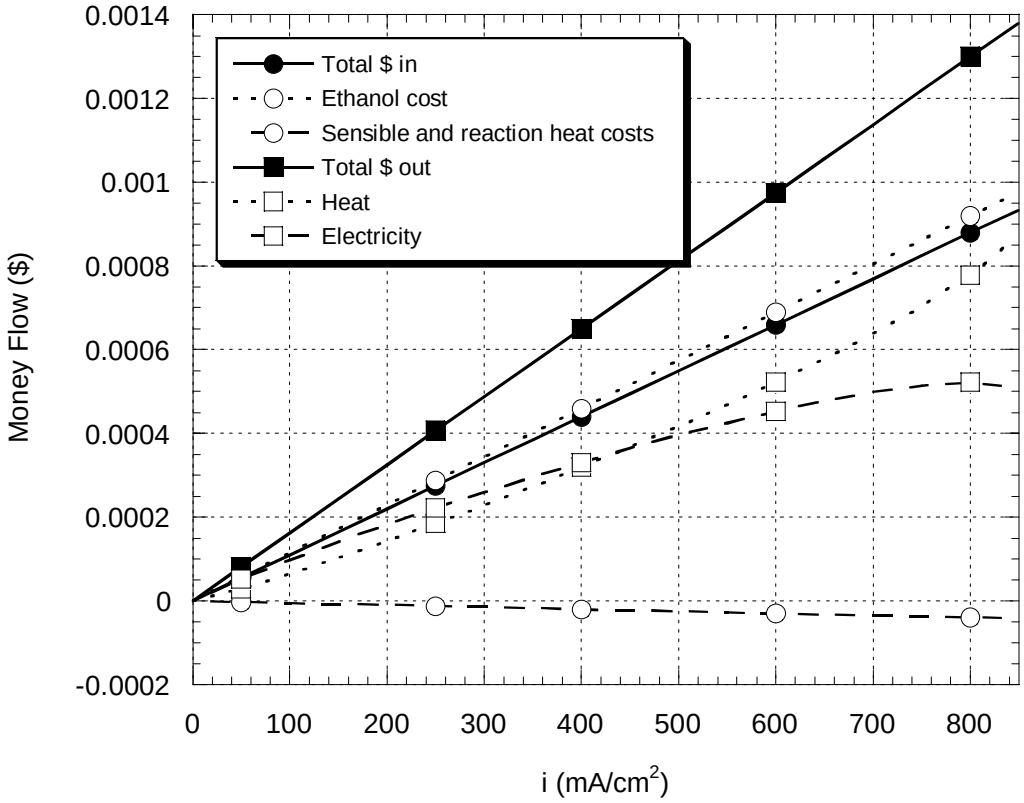


***Figure A.4.*** *Money flow scheme for a system of an ethanol autothermal reformer and a small PEM cell of area 10 cm$^2$ (See text for details.)*

bioethanol to produce ethanol. On the other hand, heat generated in the fuel cell has an energy value that cannot be underestimated. When the "Total $ in" and "Total $ out" curves are compared, it is observed that a profit of about 37% and 48% can be made out of such a system using a steam reformer and an autothermal reformer, respectively. Interestingly, it has been shown by recent studies that the energy in the fuel ethanol is at least 1.34 times the energy used in its production which is quite near to the values obtained here [7]. Yet, however, to remain on the profitable side, electricity price/cost should not fall below $0.09/kWh for both reformers. At this value operating cost becomes almost the same as the selling price of the electricity at which point, though, operating such

a system would be meaningless. Therefore, the fuel cost at the end of this analysis came out to be $0.09/kWh which is more than twice of the fuel cost estimated by Deluga et al. [7]. Still, this value will decrease if bioethanol can be used instead of pure ethanol which can supply even more than the amount of water necessary to drive the steam reforming reaction.

One more point should be made clear: Figures A.3 and A.4 show the results for a cell of 10 $cm^2$ electrode. Increase or decrease in this value only shifts the curves up or down, respectively, unchanging the profit ratio since all calculations are linear multiplication of data.

# APPENDIX B

## CATALYST PREPARATION AND CHARACTERIZATION

*Preparation of Set I Catalysts*

Contents here were obtained from Assist. Prof. Dr. Erol Şeker and Işıl Tezel at Izmir Institute of Technology. This information is presented here for the completeness of the study.

Promoted and non-promoted ZnO catalysts supported on silica were prepared by a single-step sol-gel technique based on the technique of Brinker et al. [47]:

***Table A.4.*** *Amounts used in preparation of Set I catalysts*

| Species | Samples | | | | | |
|---|---|---|---|---|---|---|
| | **1** | **2** | **3** | **4** | **5** | **6** |
| Ethanol (ml) | 4 | 4 | 4 | 4 | 4 | 4 |
| TEOS (ml) | 4 | 4 | 4 | 4 | 4 | 4 |
| Water (ml) | 0 | 0 | 0 | 1.519 | 1.519 | 2 |
| HCl (1M) (ml) | .013 | .013 | .013 | .02622 | .0065 | .013 |
| $NH_4OH$ (.05M) (ml) | .833 | .833 | .833 | .833 | .833 | .350 |
| $Zn(NO_3)_2.6H_2O$ (g) | 3.7760 | 3.7792 | 3.7775 | 3.7740 | 3.7703 | 3.7750 |
| $Cu(NO_3)_2.2H_2O$ (g) | .4637 | .3321 | 0 | 0 | 0 | 0 |
| $Pd(NO_3)_2.H_2O$ | 0 | 0 | .1190 | 0 | 0 | 0 |

Tetraethylorthosilicate (TEOS) was firstly dissolved in ethanol. Temperature of the resulting solution was raised to 65°C, and diluted hydrochloric acid was added into the solution. Stirred continuously by a magnetic stirrer this solution was kept at 65°C in a vessel equipped with a total reflux for 3 hours. Meanwhile for the preparation of non-promoted catalysts, $Zn(NO_3)_2.6H_2O$ was dissolved in $NH_4OH$ at 65°C. This basic solution was added into previously prepared acidic solution and stirred continuously at 65°C until gel formation was observed. In a similar manner, for the preparation of Cu and Pd promoted catalysts $Zn(NO_3)_2.6H_2O$ was dissolved in $Cu(NO_3)_2.2H_2O$ and $Pd(NO_3)_2.H_2O$, respectively, to prepare the basic solution which was then added into acidic solution until the formation of gel. Table A.4 summarizes the amounts used during preparation. Gels were then dried under vacuum for three days.

*Preparation of Set II Catalyst*

Set II catalysts were prepared at Chemistry Department of METU under the supervision of Assist. Prof. Dr. Ayşen Yılmaz. Information here was obtained from Burcu Akça and given here for the completeness of the study.

A triblock co-polymer, P123 ($EO_{20}PO_{70}EO_{20}$)[12], was dissolved in hydrochloric acid under continuous stirring by magnetic stirrer at room temperature for one hour. TEOS, as the silica source, and $CoCl_2.6H_2O$, as the cobalt source, were added into the mixture at 40°C. The resulting solution was again stirred continuously for about 20 hours until gel formation was observed. Then gels were dried overnight at 90-100°C, and filtered afterwards.

*Catalyst Characterization*

Calcination procedure of Set I catalysts was determined by means of TGA technique (DuPont 2000) in Chemical Engineering Department at METU.

[12] Triblock poly(ethyleneoxide)-poly(propeleneoxide)-poly(ethyleneoxide) co-polymer

Appendix C presents TGA data for samples 1, 3 and 5, and the calcination procedure performed for each Set I catalyst.

After calcination of Set I catalysts they were ground in mortar to 60 mesh size. On the other hand, Set II catalyst was calcined directly at 500°C for two hours and used without grinding.

BET surface areas and average pore diameters of some of SET I catalysts and Set II catalyst were determined by nitrogen adsorption in Coulter Omnisorp 100 at Izmir Institute of Technology and in Micromeritics ASAP 2000 at METU, respectively.

# APPENDIX C

# CALCINATION PROCEDURES AND TGA DATA OF SET I CATALYSTS

***Table A.5.*** *Calcination procedures of Set I catalysts*

| Sample | Calcination Procedure |
|---|---|
| 1, 2, 4, 5, 6 | *RT* [10°C/min] *150℃* (1h) [10°C/min] *350℃* (1h) [3°C/min] *450℃* (1h) [10°C/min] *500℃* (1h+3h[13]) |
| 3 | *RT* [10°C/min] *150℃* (1h) [3°C/min] *200℃* (1h) [10°C/min] *350℃* (1h) [10°C/min] *500℃* (1h+3h[13]) |

[13] After one hour at 500°C, samples were weighed and kept for another 3 hours at 500°C after which samples were weighed once again. As there were no significant weight differences calcination of samples was completed.

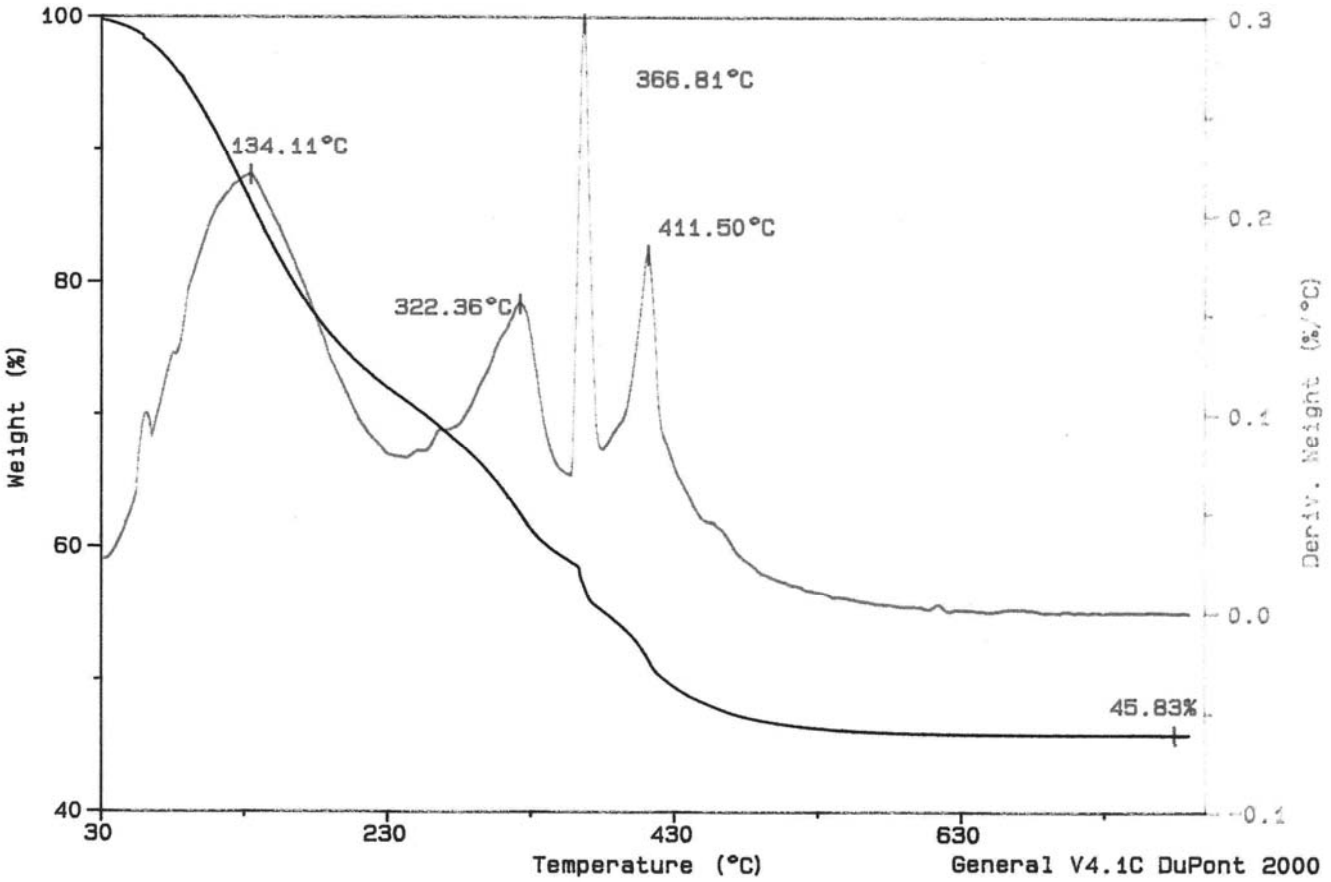


***Figure A.5.*** *TGA of sample 1 (RT [10 ℃/min] 700 ℃. Air flow: 75 $cm^3$/min.)*

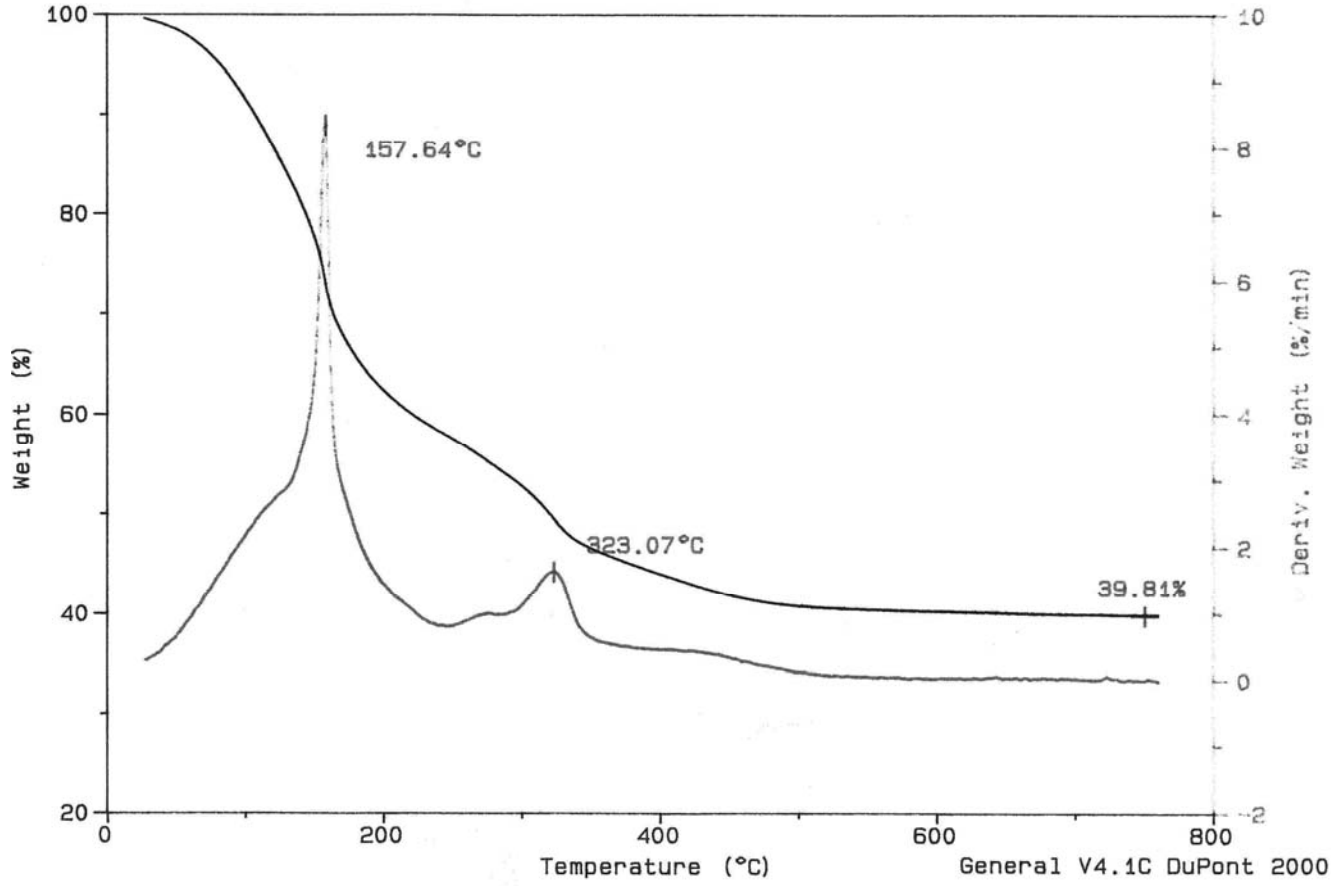


***Figure A.6.*** *TGA of sample 3 (RT [10 ℃/min] 700 ℃. Air flow: 60 $cm^3$/min.)*

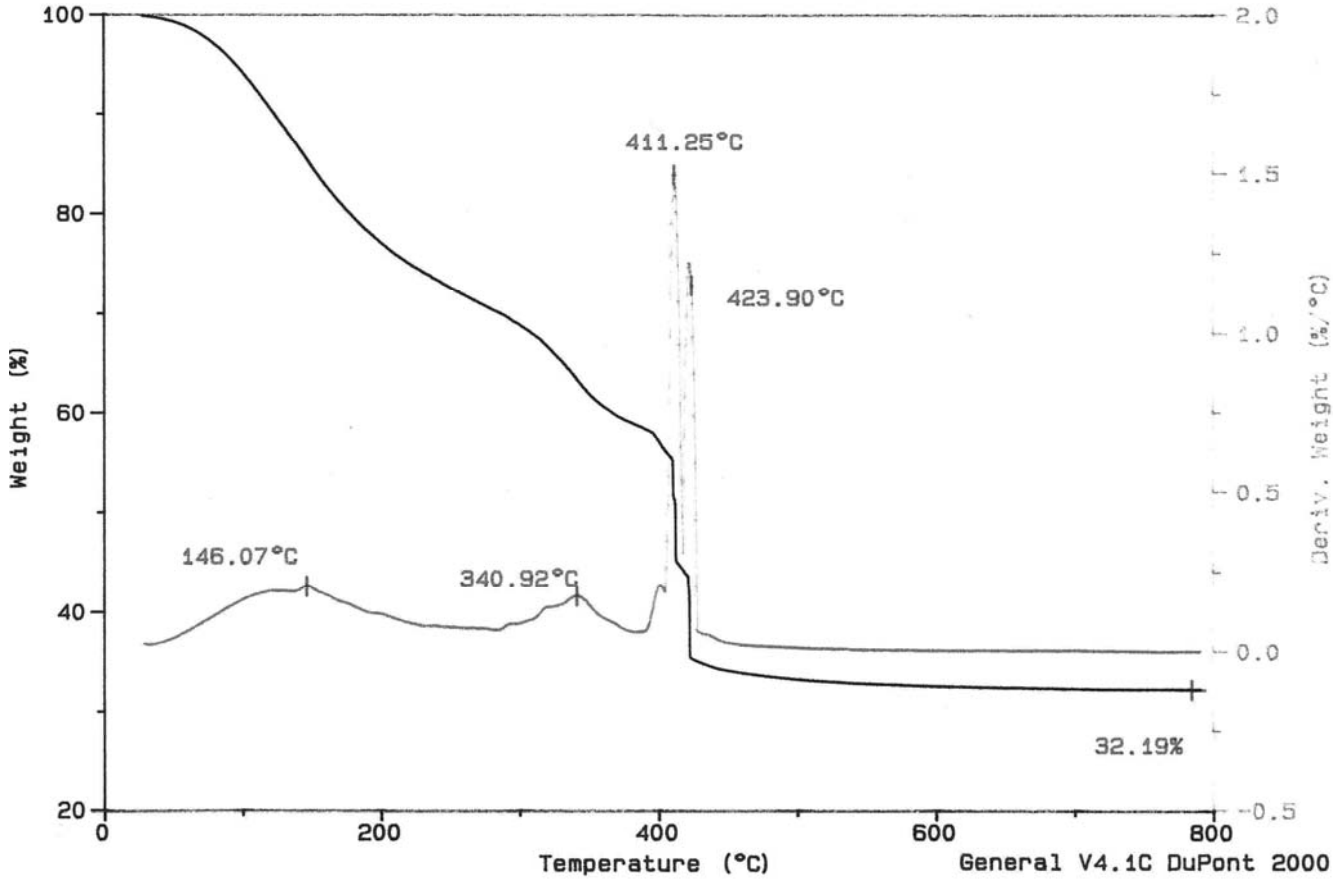


***Figure A.7.*** *TGA of sample 5 (RT [10 ℃/min] 700 ℃. Air flow: 75 $cm^3$/min.)*

# APPENDIX D

## ELEMENTAL CARBON BALANCES IN STEAM REFORMING TESTS

Acetaldehyde and ethanol are the only carbon-containing species encountered in ethanol steam reforming experiments. Amount of ethanol, and thus that of elemental carbon, fed to the system was obtained from the analysis of the effluent obtained at the "no reaction" temperature, 200°C. This value was then compared with the amount of elemental carbon in other reaction temperatures.

***Table A.6.*** *Percent errors in elemental carbon balances (Fresh catalysts. S: Same-day calibration data. A: Averaged calibration data.)*

| Sample | T (°C) → | 300 | 350 | 400 | 450 | 500 |
|---|---|---|---|---|---|---|
| 1 | S | +5.9 | +9.0 | -11.5 | -1.7 | -3.9 |
| | A | -9.3 | +6.8 | -25.1 | -21.3 | -22.8 |
| 2 | S | +9.3 | +15.7 | -6.1 | -10.1 | -18.6 |
| | A | +2.1 | +7.1 | -24.5 | -27.1 | -51.0 |
| 3 | S | +12.4 | +6.8 | +14.0 | +22.3 | +32.5 |
| | A | +12.4 | +6.0 | +11.5 | +11.1 | +19.5 |
| 4 | S | -0.2 | +0.4 | -11.1 | -5.1 | N/A |
| | A | +27.9 | +17.0 | -15.8 | -3.2 | N/A |
| 6 | S | 0 | -10.0 | -51.1 | -89.0 | -120.5 |
| | A | -11.9 | -15.4 | -52.6 | -49.2 | -45.6 |

Results are summarized in Table A.6. A positive figure can be expressed as a "carbon *consumption* or accumulation," and a negative figure as a "carbon *generation*."

# APPENDIX E

## AVERAGED CALIBRATION DATA

For steam reforming experiments, peak areas of components were related to their corresponding flow rates through same-day calibration data obtained from argon areas (necessary for the determination of total gas flow rate) and single-point calibrations done for every component in each experiment. All such area-to-mol/min calibration data were collected and their slopes were calculated (area/flow rate). 95% confidence level intervals of those slopes were then computed from their average values and standard deviations. The area and flow rate data giving those slopes falling in that interval were selected, and from these data area-to-mol/min calibration curves were plotted. These plots are given in Figures A.8-A.13[14].

It should be carefully noted that these plots are not calibration curves obtained simply by sending a gas at some flow rate to GC and obtaining the peak area. First of all, they all include experimental data of steam reforming experiments which were quantified by single-point calibration and in which effect of temperature was included by argon peak area. Temperature affects the total flow rate, and hence, the argon area, in two ways: 1. If there were no reaction taking place, increase in temperature would accelerate the gas molecules. 2. There are reactions taking place differently at different temperatures so total flow rate will be different at each temperature[15]. Therefore, these data are termed as "averaged" in the text because they were obtained at five different experimental temperatures between 300-500°C and they were applied to every other raw data

[14] IS in figure titles stands for "internal standard" which is argon.
[15] Flow rate increased with temperature in steam reforming tests as two molecules were produced from one molecule of ethanol in the only reaction taking place, ethanol dehydrogenation.

(peak areas) which have no argon data disregarding the temperature. These plots are, thus, temperature-corrected calibration curves.

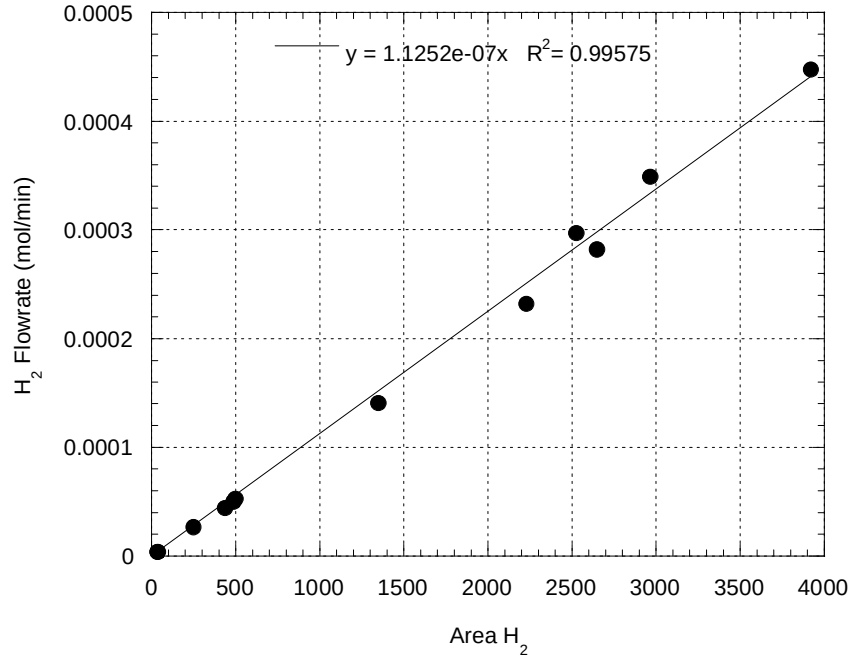


***Figure A.8.*** *Effect of temperature on quantification of hydrogen via an IS*[14]

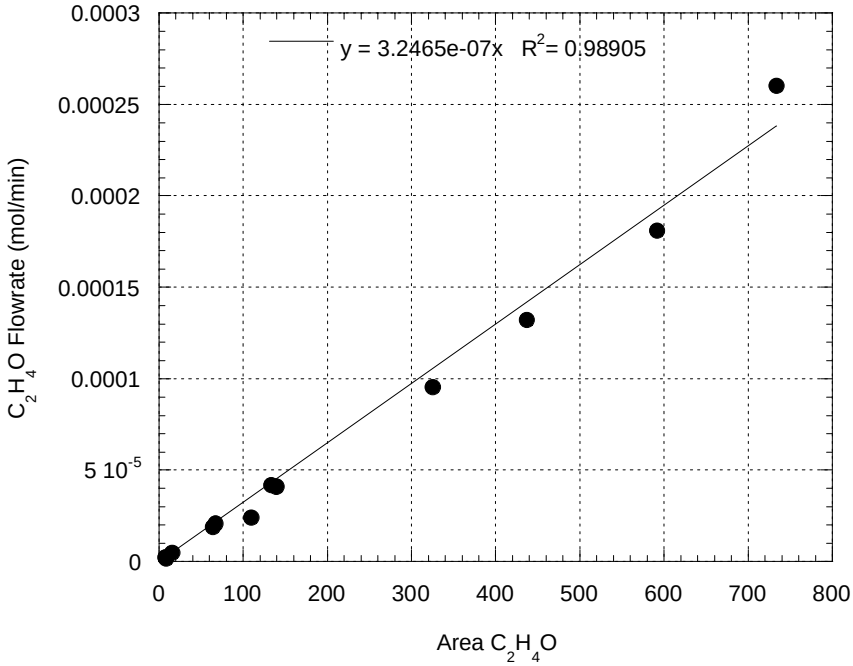


***Figure A.9.*** *Effect of temperature on quantification of acetaldehyde via an IS*[14]

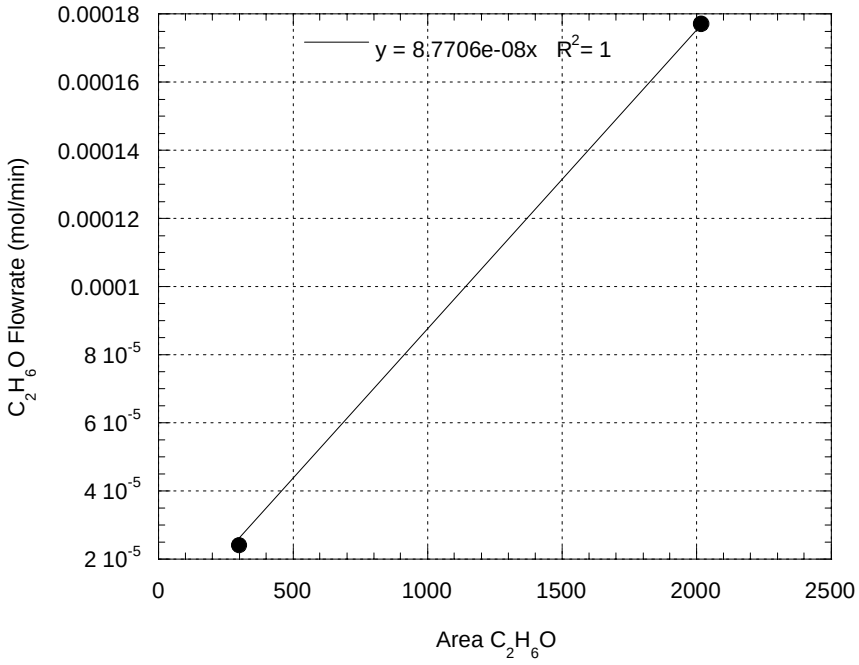


***Figure A.10.*** *Effect of temperature on quantification of ethanol via an IS*[14]

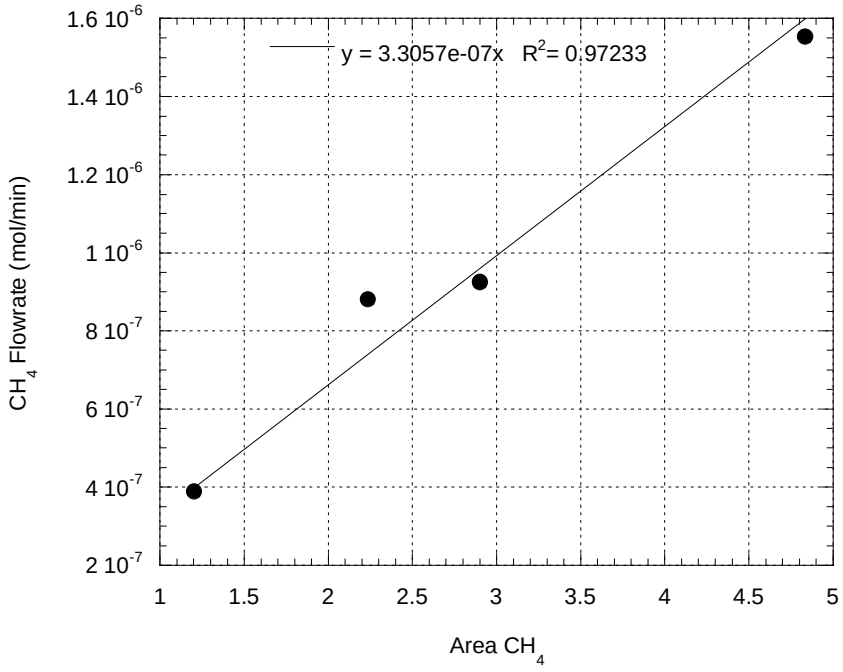


***Figure A.11.*** *Effect of temperature on quantification of methane via an IS*[14]

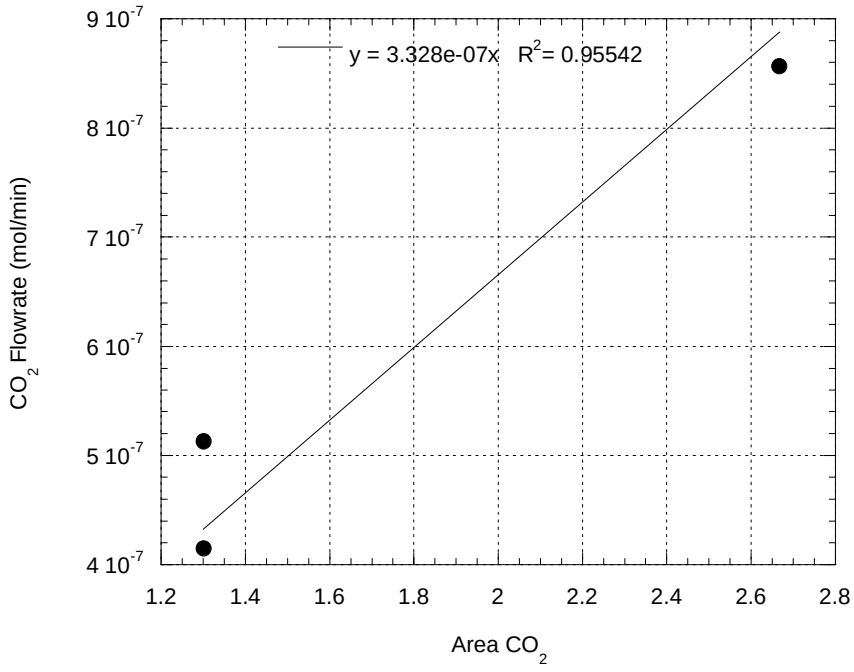


***Figure A.12.*** *Effect of temperature on quantification of $CO_2$ via an IS*[14]

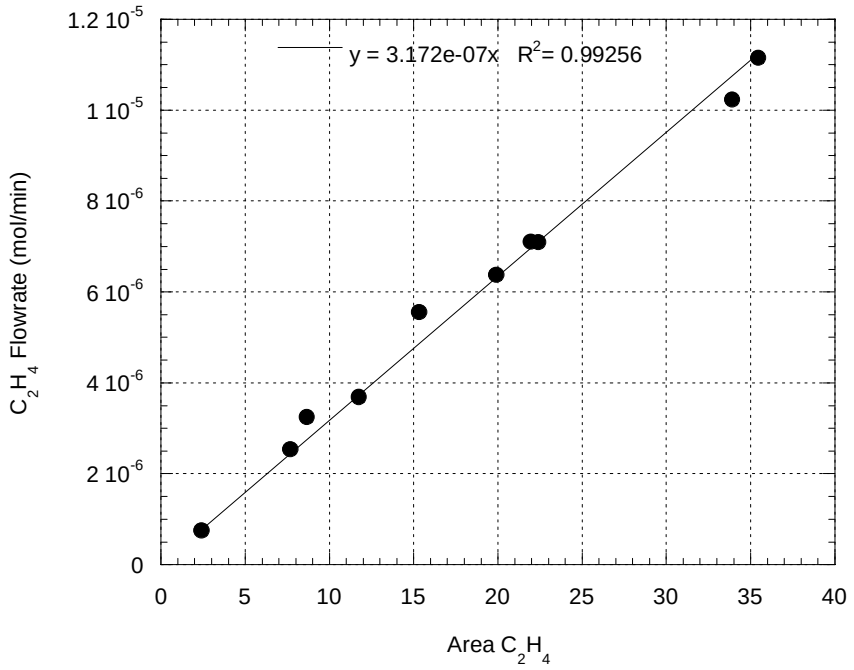


***Figure A.13.*** *Effect of temperature on quantification of ethylene via an IS*[14]

# APPENDIX F

# SAMPLE EXPERIMENTAL PROCEDURE

***Table A.7.*** *Sample experimental procedure*

| **Reactor Temperature (°C)** | **GC Analysis** | **Duration (min)** | **Time** 8:30 |
|---|---|---|---|
| 200 (No liquid feed) | Steady state in GC | 120 | 10:30 |
| 200 (No liquid feed) | Ar calibration | 40 | 11:10 |
| 200 | Ar calibration | 15 | 11:25 |
| 200 | $C_2H_4O$ calibration | 55 | 12:20 |
| 200 | $C_2H_6O$-$H_2O$ calibration | 60 | 13:20 |
| 200 | $C_2H_4O$ calibration | 55 | 14:15 |
| 200 | Effluent for 200°C | 60 | 15:15 |
| 200 | Effluent for 200°C | 60 | 16:15 |
| 300 | Effluent for 200°C | 60 | 17:15 |
| 300 | $H_2$ calibration | 60 | 18:15 |
| 300 | Effluent for 300°C | 60 | 19:15 |
| 300 | Effluent for 300°C | 60 | 20:15 |
| 350 | Effluent for 300°C | 60 | 21:15 |
| 350 | $C_2H_6O$-$H_2O$ calibration | 60 | 22:15 |
| 350 | Effluent for 350°C | 60 | 23:15 |
| 350 | Effluent for 350°C | 60 | 0:15 |
| 400 | Effluent for 350°C | 60 | 1:15 |
| 400 | Effluent for 400°C | 60 | 2:15 |
| 400 | Effluent for 400°C | 60 | 3:15 |
| 450 | Effluent for 400°C | 60 | 4:15 |
| 450 | Effluent for 450°C | 60 | 5:15 |
| 450 | Effluent for 450°C | 60 | 6:15 |
| 500 | Effluent for 450°C | 60 | 7:15 |
| 500 | Effluent for 500°C | 60 | 8:15 |
| 500 | Effluent for 500°C | 60 | 9:15 |
| Shutting down | Effluent for 500°C | 60 | 10:15 |
| Shutting down | Calibration gas | 55 | 11:10 |
| Shutting down | Shutting down | 60 | 12:10 |
| Total Time | | 1660 min (27.7 h) | |

# APPENDIX G

## SETUP PICTURES

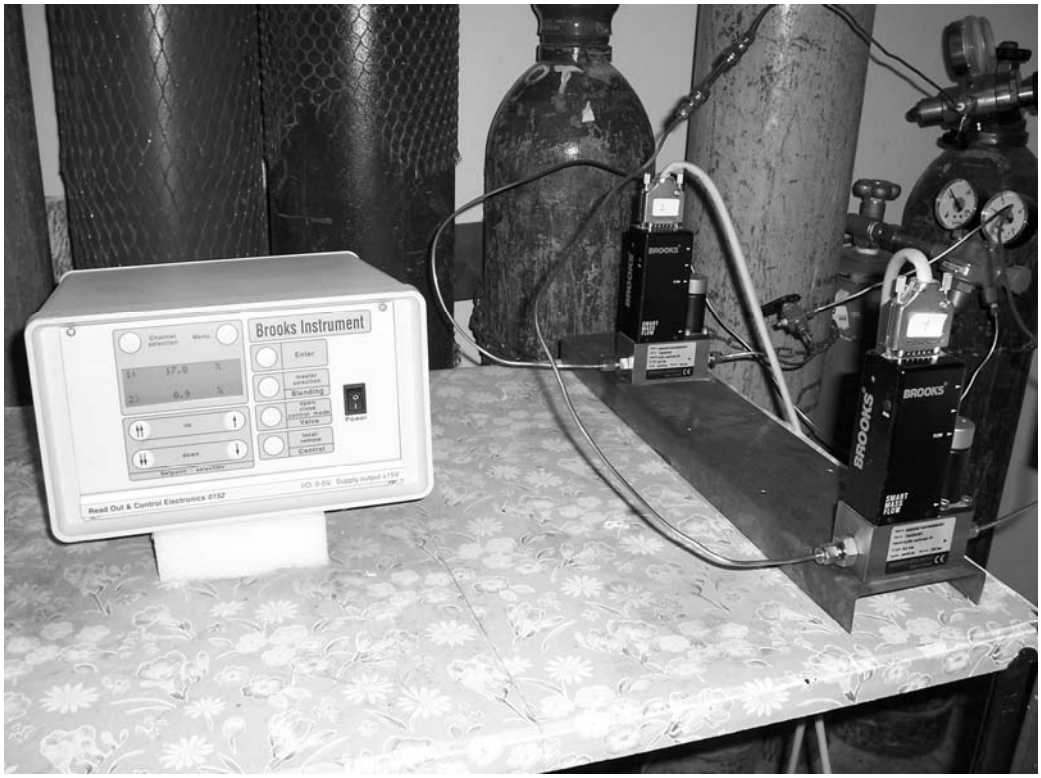


***Figure A.14.*** *Gas cylinders and mass flow controllers*

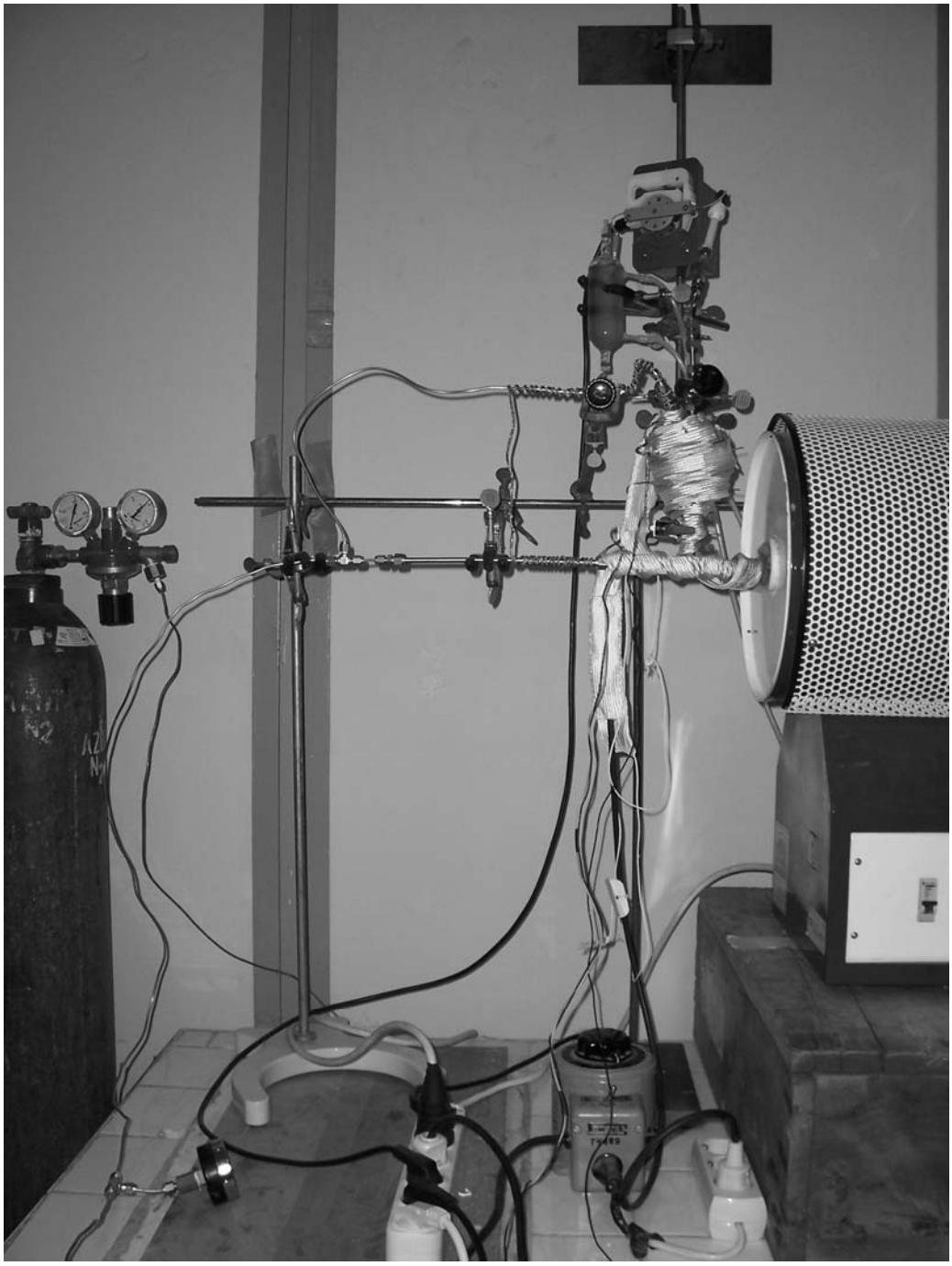

***Figure A.15.*** *Feeding unit*

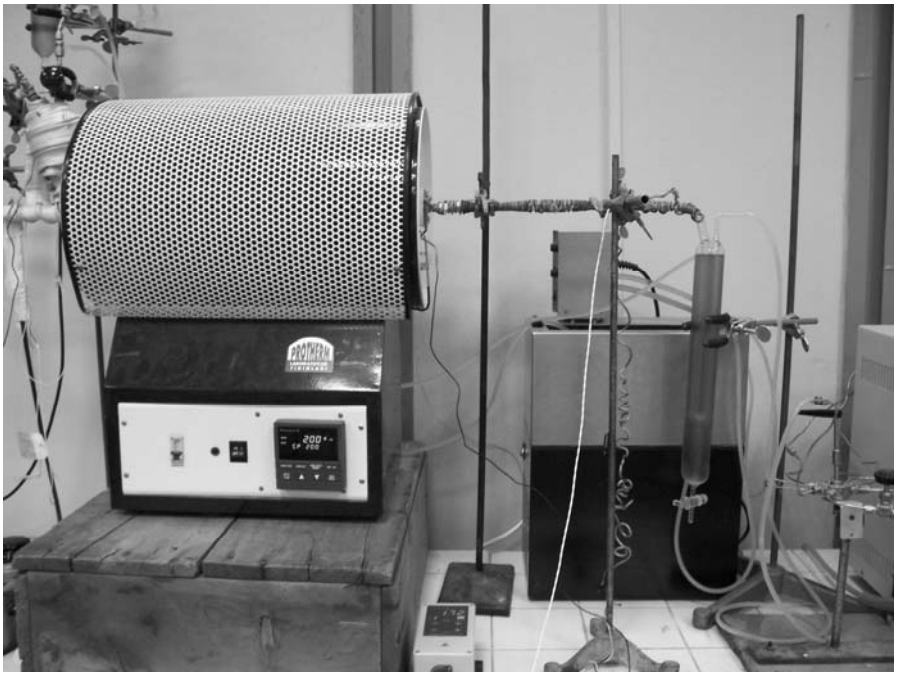

***Figure A.16.*** *Reacting unit*


***Figure A.17.*** *Analyzing unit (GC)*

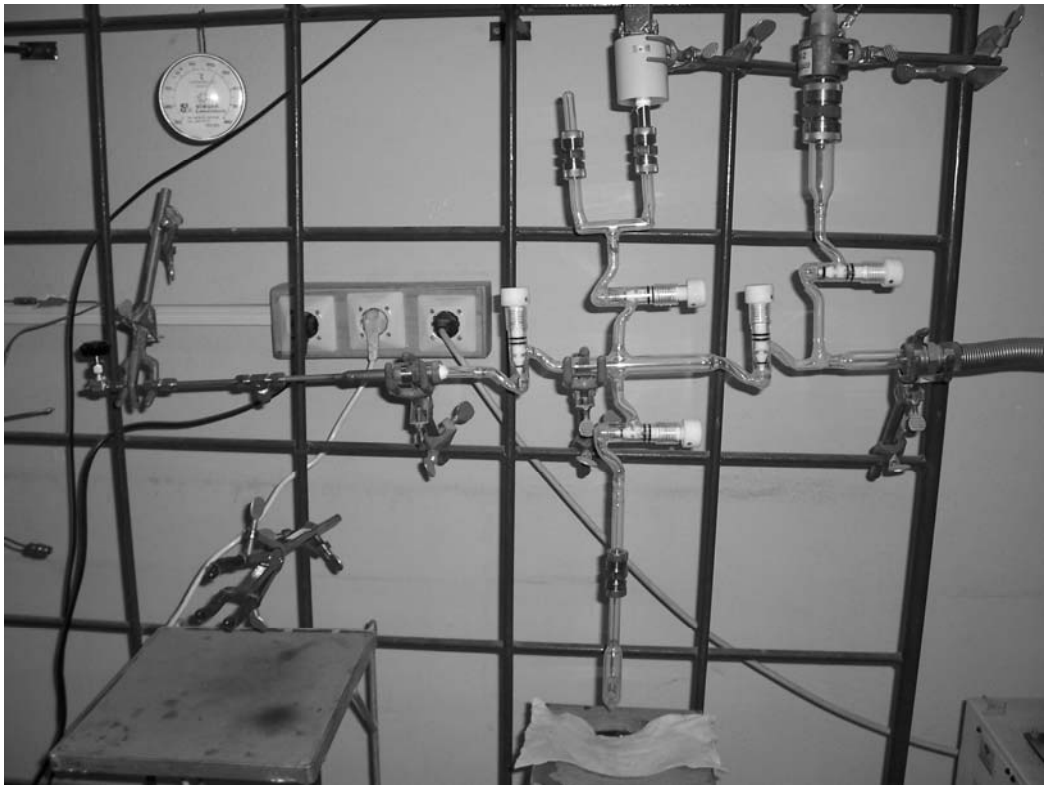

***Figure A.18.*** *Manifold used in gas calibrations*